

POLYMER FUNCTIONALIZATION OF
SINGLE-WALLED CARBON NANOTUBES

POLYMER FUNCTIONALIZATION OF SINGLE-
WALLED CARBON NANOTUBES USING LIVING
POLYMERIZATION METHODS

By

YUANQIN LIU, B.Sc., M.Sc.

A Thesis

Submitted to the School of Graduate Studies

In Partial Fulfillment of the Requirements

For the Degree

Master of Science

McMaster University

© Copyright by Yuanqin Liu, August 2004

MASTER OF SCIENCE (2004)
(Chemistry)

McMaster University
Hamilton, Ontario

TITLE: Functionalization of Single-Walled Carbon Nanotubes
using Living Polymerization Methods

AUTHOR: Yuanqin Liu, B.Sc., M.Sc.

SUPERVISOR: Professor Alex Adronov

NUMBER OF PAGES: xii, 82

Abstract

Single-walled carbon nanotubes (SWNTs) were oxidatively shortened and functionalized with ruthenium-based olefin metathesis catalysts. These catalyst-functionalized nanotubes were shown to be effective in the ring-opening metathesis polymerization of norbornene, resulting in rapid polymerization from the catalyst sites on the nanotube. It was found that high polymer molecular weights could be reached, and the molecular weight increased linearly with polymerization time. The resulting polynorbornene-functionalized nanotubes were found to exhibit solubility in organic solvents, while the starting materials and catalyst-functionalized nanotubes were completely insoluble. The polymerized materials were characterized by NMR, IR, DSC, AFM and TEM.

Polystyrene and poly[(t-butyl acrylate)-b-styrene] with well-defined molecular weights and polydispersities were prepared by nitroxide-mediated free-radical polymerization. The homo- and block-copolymers were used to functionalize shortened single-walled carbon nanotubes (SWNTs) through a radical coupling reaction involving polymer-centered radicals generated at 125°C via loss of the stable free-radical nitroxide capping agent. The resulting polymer-SWNT composites were fully characterized and were found to be highly soluble in a variety of organic solvents. This solubility could also be altered through chemical modification of the appended polymers. The t-butyl groups of appended

PtBA-b-PS could be removed to produce poly[(acrylic acid)-b-styrene]-functionalized carbon nanotubes. The resulting composite was found to form aggregates in a mixture of chloroform/methanol (v/v: 1/1), as determined by dynamic light scattering (DLS).

Acknowledgements

I would like to give my great appreciation to my supervisor, Dr. Alex Adronov for what he did for me in the past two years. He is not only a nice teacher but also a good friend who is easy to work with. Besides chemistry there are much more I can learn from him. I also want to thank Dr. Harald D.H. Stöver for his kindness and assistance during my study. They are two of the best faculty I ever met.

My thanks also go to all of my group-mates, especially Zhaoling Yao, who gave me so many help in my work.

One more important person I wish to appreciate is my wife, Ying Sun, who is my super lucky star. All of my reactions didn't show any good results before her arriving.

This work was supported by grants from the Natural Science and Engineering Research Council of Canada (NSERC), the Canada Foundation for Innovation, the Ontario Innovation Trust, as well as McMaster University. Support in the form of a Premier's Research Excellence Award is also gratefully acknowledged. Additionally, I would like to thank Frank Gibbs for thermal analysis data, Bernard Pointner and Prof. A. Vreugdenhil (Trent University) for the Raman spectroscopy data, Todd Hoare for the light scattering measurements, Nadi Braidy and Prof. G. A. Botton for TEM data, Prof. Gillian R. Goward and Lindsey Cahill for solid-state NMR data, as well as Andy Duft for AFM measurement.

TABLE OF CONTENTS

	Page
<u>ABSTRACT</u>	iii
<u>ACKNOWLEDGEMENTS</u>	v
<u>TABLE OF CONTENTS</u>	vi
<u>LIST OF SCHEMES</u>	ix
<u>LIST OF FIGURES</u>	x
Chapter 1: INTRODUCTION.....	1
1.1 Introduction of Single-Walled Carbon Nanotubes (SWNTs)	1
1.1.1 Synthesis of SWNTs	2
1.1.2 Properties of SWNTs	3
1.1.3 Potential Applications of SWNTs	5
1.2 Chemical Functionalization of SWNTs	6
1.3 Ring-Opening Metathesis Polymerization (ROMP)	8
1.4 Stable Free Radical Polymerization (SFRP).....	9
1.5 Radical Coupling Chemistry.....	11
Chapter 2: OBJECTIVES	13
2.1 Polymer Functionalization of SWNTs via ROMP.....	13
2.2 Functionalization of SWNTs via Radical Coupling Chemistry.....	14
Chapter 3: FUNCTIONALIZATION of SWNTs using ROMP	15
3.1 Overview.....	15
3.1.1 Shortening and Purification of SWNTs	15

3.1.2 Synthesis and Characterization of End Polynorbornene-Functionalized SWNTs.....	18
3.1.3 Synthesis and Characterization of Side Wall Polynorbornene-Functionalized SWNTs.....	36
3.2 Experimental	43
General.....	43
Shortening and Purification of SWNTs	44
Synthesis of end triol-functionalized SWNTs (3).....	45
Synthesis of end norbornene-functionalized SWNTs (5).....	45
Synthesis of end catalyst-functionalized SWNTs (7).....	46
General procedure for ring-opening metathesis polymerization using the end catalyst-functionalized SWNT macroinitiator (7).....	46
General procedure for cleavage of polynorbornene from the end polynorbornene-functionalized SWNTs (8).....	47
Synthesis of side-wall phenol-functionalized SWNTs (9).....	48
Synthesis of side-wall vinyl-functionalized SWNTs (10).....	48
Synthesis of side-wall catalyst-functionalized SWNTs (11).....	48
General procedure for ring-opening metathesis polymerization using the side-wall catalyst-functionalized SWNT macroinitiator (11).....	49

Chapter 4: FUNCTIONALIZATION of SWNTs using

RADICAL COUPLING CHEMISTRY.....	50
4.1 Overview.....	50
4.1.1 Functionalization of shortened SWNTs with PS.....	50
4.1.2 Functionalization of shortened SWNTs with Diblock Polymers...	62
4.1.3 SWNTs Functionalized with Amphiphilic Block Copolymers.....	66
4.2 Experimental	70
General.....	70
Shortening and Purification of SWNTs	72

Synthesis of polystyrene (14).....	72
Synthesis of poly(t-butyl acrylate) (PtBA) (17).....	73
Synthesis of poly[(t-butyl acrylate)-b-styrene] (18).....	74
Synthesis of PtBA-b-PS functionalized SWNTs (19).....	74
Formation of poly(acrylic acid-b-styrene) functionalized SWNTs (20).....	74
 Chapter 5: CONCLUSIONS.....	 75
 REFERENCES.....	 76

List of Schemes

	Page
Scheme 1. General mechanism of ROMP	8
Scheme 2. General mechanism for 2,2,5,5-tetramethyl-3-(1-phenylethoxy) -4-chloromethyl-phenyl-3-azahexane 1 initiated SFRP	10
Scheme 3. Functionalization of fullerenes with polymer via free radical polymerization.....	11
Scheme 4. Grafting from approach using ROMP	13
Scheme 5. Grafting to approach using radical coupling chemistry	14
Scheme 6. Shortening and purification of SWNTs	16
Scheme 7. Synthesis of end triol-functionalized nanotubes (3).....	19
Scheme 8. Synthesis of end catalyst-functionalized nanotubes (7).....	20
Scheme 9. ROMP from SWNTs	23
Scheme 10. Defunctionalization of end functionalized polynorbornene- SWNT composites.....	32
Scheme 11. Synthesis of side-wall catalyst functionalized SWNTs (11)..	38
Scheme 12. ROMP from side wall of SWNTs	40
Scheme 13. (A) Preparation of PS by nitroxide mediated “living” free- radical polymerization and (B) Functionalization of SWNTs by nitroxide-terminated PS	51
Scheme 14. Preparation of PtBA-b-PS by nitroxide mediated “living” free-radical polymerization, and its utilization for the functionalization of SWNTs	62
Scheme 15. Deprotection of PtBA-b-PS functionalized SWNTs to produce PAA-b-PS functionalized SWNTs	68

List of Figures

	Page
Figure 1. Indexing scheme that shows the folding procedure to create nanotube cylinders from planar graphene sheets.	4
Figure 2. AFM images of (A) Pristine SWNTs, and (B) shortened SWNTs.....	17
Figure 3. IR spectra of (A) compounds 1 , (B) 3 , (C) 5 , (D) 7 , (E) 8	22
Figure 4. Raman spectra of (A) shortened nanotubes, and (B) end polynorbornene-functionalized nanotubes.....	24
Figure 5. Samples of (A) shortened, unfunctionalized nanotubes 1 , (B) end catalyst-functionalized nanotubes 7 and (C) polymerized nanotubes 8 in THF.....	25
Figure 6. UV/ Vis spectra of (A) mixture of polynorbornene and shortened nanotubes, and (B) end polynorbornene-functionalized nanotubes.....	26
Figure 7. Calibration curve of SWNTs made in by Smalley	26
Figure 8. ¹ H NMR spectra of (A) polynorbornene and (B) polynorbornene-functionalized nanotubes.....	27
Figure 9. ¹³ C NMR spectra of (A) polynorbornene and (B) polynorbornene-functionalized nanotubes.....	28
Figure 10. AFM images of nanotubes before (A) and after (B) polymerization. Two close-ups of individual structures, (C) and (D).....	30
Figure 11. TEM image of end polymer-functionalized nanotubes.....	31
Figure 12. ¹ H NMR spectra of (A) polynorbornene and (B) cleaved polynorbornene.....	33
Figure 13. Plot of the molecular weight and polydispersity of polynorbornene cleaved from the SWNTs as a function of polymerization time.	33

Figure 14. DSC traces of (A) unfunctionalized carbon nanotubes, (B) polynorbornene functionalized nanotubes and (C) cleaved polynorbornene	35
Figure 15. TGA traces of polynorbornene functionalized nanotubes.....	36
Figure 16. IR spectra of (A) compounds 1 , (B) 9 , (C) 10 , (D) 11 , (E) 12	39
Figure 17. Raman spectrum for the side wall polynorbornene functionalized SWNTs (12).....	40
Figure 18. AFM images of (A) side wall polynorbornene functionalized SWNTs (12) and (B) the profile traces at different points along the features are given	41
Figure 19. TEM image of side wall polynorbornene functionalized SWNTs (12).....	42
Figure 20. GPC results of a typical PS prepared by “living” free-radical polymerization utilizing alkoxyamine initiator.....	52
Figure 21. Shortened SWNTs in CH ₂ Cl ₂ /H ₂ O (A) and PS functionalized SWNTs in various solvents: CH ₂ Cl ₂ /H ₂ O (B), THF (C), CHCl ₃ (D).....	53
Figure 22. Solid-state ¹ H NMR spectra of (a) shortened unfunctionalized SWNTs and (b) initiator-functionalized SWNTs	54
Figure 23. Optical density at 500 nm of shortened SWNTs in H ₂ O at different concentrations.....	56
Figure 24. UV/Vis spectra of (A) shortened SWNTs in H ₂ O and (B) PS functionalized SWNTs in THF (saturated solutions were diluted 10-fold prior to measurement).....	56
Figure 25. ¹ H NMR spectra of (A) PS and (B) PS functionalized SWNTs.	57
Figure 26. Raman spectra of (A) shortened SWNTs and (B) PS functionalized SWNTs.....	59

Figure 27. AFM image of purified SWNTs (A); AFM image of PS functionalized SWNTs spin-cast from THF solution (B); AFM image of PS functionalized SWNTs spin-cast from CHCl ₃ solution (C); TEM image of PS functionlized SWNTs (D).....	61
Figure 28. TGA traces of (A) PS and (B) PS functionalized SWNTs.....	62
Figure 29. ¹ H NMR spectra of PtBA-b-PS (A) and PtBA-b-PS functionalized SWNTs (B).....	65
Figure 30. TGA data (A) and DSC data (B) for PtBA-b-PS (i) and PtBA-b-PS functionalized SWNTs (ii).....	65
Figure 31. ¹ H NMR spectra of (A) solution of PAA-b-PS functionalized SWNTs in CDCl ₃ /CD ₃ OD (v/v: 3/1) and (B) micelle of PAA-b-PS functionalized SWNTs in CDCl ₃ / CD ₃ OD (v/v: 1/1).....	68
Figure 32. DLS data of PAA-b-PS functionalized SWNTs particles in CHCl ₃ /MeOH	70

Chapter 1 Introduction

1.1 Introduction to Single-Walled Carbon Nanotubes (SWNTs)

Since they were first discovered by Ijima and coworkers in 1990's,^{1,2} carbon nanotubes which include single walled carbon nanotubes (SWNTs) and multi walled carbon nanotubes (MWNTs) have attracted much attention due to their unique structural, physical, chemical and electronic properties. Their unique properties position them as one of the leading materials for a wide array of potential nanotechnological applications, such as molecular wires and electronics,^{3,4} sensors,⁵ high-strength fibers,⁶ and field emission.⁷ However, there are several fundamental disadvantages that prohibit the expansion of their applications. Those challenges include high production cost, low product purity, difficulty to separate by chirality and insolubility.⁸⁻¹²

As part of the ongoing progress towards expanding their utility, the preparation of carbon nanotube derivatives, through chemical modification, has been the subject of intense recent interest.¹³ However, most chemical reactions happen in solution while SWNTs are highly insoluble in all known solvents. Thus one of the main goals of this work is the improvement of nanotube solubility in various organic and aqueous solvents, as well as their miscibility with bulk materials, such as polymers.¹⁴ Recently, many publications reported that functionalized SWNTs can be dissolved in both organic and aqueous media.¹⁵⁻²³

Now it is possible to characterize, study the properties, and utilize the potential applications of carbon nanotubes using solution-based techniques.

1.1.1 Synthesis of SWNTs

Arc discharge,^{1,11,24} laser ablation,¹⁰ chemical vapour deposition (CVD),²⁵⁻²⁸ pyrolysis,^{29,30} and high pressure carbon monoxide disproportionation (HiPco)³¹ are the main methods used for carbon nanotube synthesis. Arc discharge and laser ablation use solid state carbon precursors as carbon sources and involve carbon vaporization at high temperature. CVD employs hydrocarbon gases to provide carbon sources and metal catalyst particles to serve as “seeds” needed for nanotube growth. A relatively lower temperature is needed for this approach. Another convenient approach by which carbon nanotubes can be obtained is the pyrolysis of organometallic precursors such as metallocenes and phthalocyanines in a reducing atmosphere. It is important that aligned nanotube bundles have been obtained from this method. With one particular method, named the HiPco process, Smalley’s group has described a scalable synthetic technique, where carbon monoxide is utilized as a feedstock. This is a gas-phase catalytic process where the catalyst (iron-metal clusters) is formed from the pyrolysis of iron pentacarbonyl, $\text{Fe}(\text{CO})_5$, at 800°C . Carbon monoxide disproportionates to form elemental carbon and CO_2 , which occurs catalytically on the surface of the iron particles, upon which SWNTs nucleate and grow. Compared to other methods, which produce SWNTs in milligram to gram quantities in a few hours, the HiPco

process can produce approximately one kilogram of SWNTs per day. However, some metal catalyst and amorphous carbon remain in the final products, which give a 90% purity and a 40% yield. This process was the source of the SWNTs used in our investigation, which are commercially available from Carbon Nanotechnologies Inc.

1.1.2 Properties of SWNTs

SWNTs are seamless structures that could be imagined as a sheet of graphene folded into a carbon cylinder such that the open edges match perfectly. (Figure 1).^{2,6,9} In the mapping of a graphene plane into a cylinder, the boundary conditions around the cylinder can be satisfied only if one of the two primitive lattice vectors (\mathbf{a}_1 , \mathbf{a}_2) of the graphene sheet maps to a whole circumference of the cylinder (Figure 1). Nanotubes made from lattice translational indices of the form $(n, 0)$ or (n, n) will have two helical symmetry operations whereas all other sets of nanotubes will have the three equivalent helical operations. The (n, n) type of nanotubes are in general called zigzag nanotubes whereas the $(n, 0)$ types are called armchair nanotubes. All others will be helical.

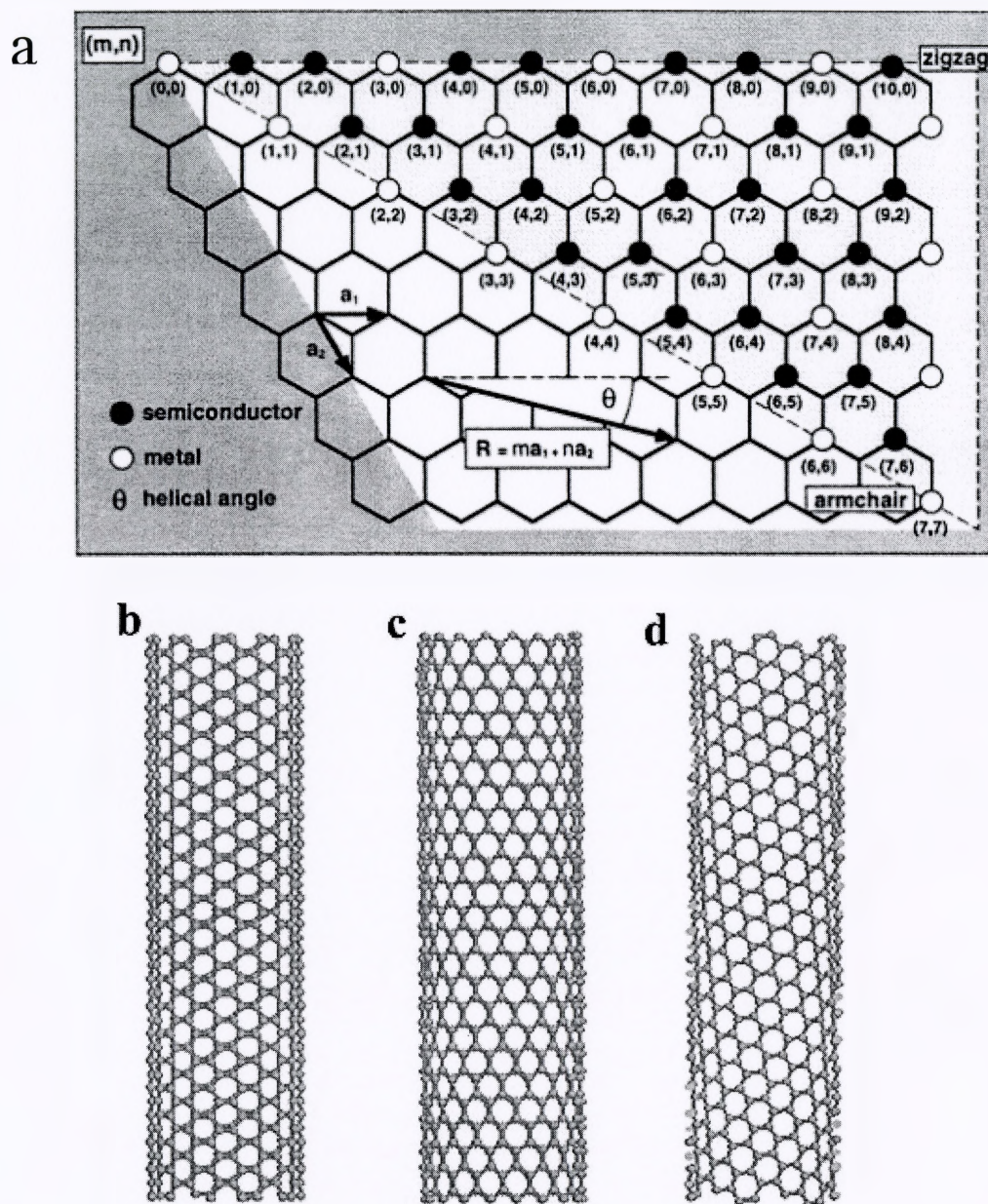


Figure 1. (a) Indexing scheme that shows the folding procedure to create nanotube cylinders from planar graphene sheets. \mathbf{a}_1 and \mathbf{a}_2 are the primitive lattice vectors of the hexagonal lattice. The position and length of the vector, \mathbf{R} , connecting an origin to the lattice point that defines the nanotube index, determine the helicity and diameter of the tube. All the (n, n) type nanotubes form armchair tubes and all $(n, 0)$ tubes are zigzag tubes. (b) armchair, (c) zigzag, (d) chiral tubes.

The combination of dimension, structure and topology translates into a whole range of distinguishing properties which makes carbon nanotubes so special. Their remarkable electronic properties have been investigated by numerous researchers over a number of years. SWNTs show a range of electrical conductivities, from metallic to semiconducting, which are dictated by the parent structure of the nanotube lattice. Their mechanical properties are equally fascinating. The strength of the sp^2 hybridized carbon bonds makes carbon nanotubes one of the strongest and stiffest materials known. The axial elastic modulus of nanotubes is around one TPa,^{32,33} which is five times stronger than steel. It has also been reported recently that they exhibit a very high thermal conductivity³⁴ and high mechanical resilience,^{35,36} which allows them to be bent without breaking.

1.1.3 Potential Applications of SWNTs

The potential utility of SWNTs in a variety of technologically important applications, such as molecular wires and electronics, sensors, high-strength fibers, and field emission is now well established. The conductivity and tensile strength⁷ properties of this new class of nanoscale materials have attracted a great deal of investigation, which has immensely expanded their scope of applicability. The development of nanoelectronics based on nanotube electronic properties is certainly a most promising area in nanotechnology. The availability of both

semiconducting and metallic nanotubes enables a wide variety of applications. Metallic nanotubes are expected to play an important role as electronic wires (molecular wires), within field emission displays.^{25,37} Further, it has been demonstrated that semiconducting SWNTs can be used as field effect transistors (FETs),^{38,39} which are essential components for next-generation computing. It is also established that their conductivity can vary by 2 to 3 orders of magnitude when they are exposed to certain gases, such as ppm level of ammonia (NH₃),⁴⁰ nitrous oxide (NO₂),⁴⁰ and oxygen (O₂)⁴¹. These results suggest that SWNTs could possibly be used as miniature chemical or biological sensors,⁴⁰⁻⁴² as a result of their unique electronic properties.⁴³

1.2 Chemical Functionalization of SWNTs

In order to expand and realize the applications of carbon nanotubes, a number of research groups have focused on the chemical functionalization of SWNTs with various organic, inorganic, and organometallic structures using both covalent and non-covalent approaches.¹³ Many of these studies focus on improving the solubility properties of nanotubes. The primary success was achieved by functionalizing carboxylic acid groups, formed at the ends and defect sites of SWNTs during oxidative purification/shortening,^{15,16} through amidation with alkyl amines such as octadecyl amine. Over the past five years, this approach has been extended to the attachment of organometallic complexes, including Vaska's complex⁴⁴ and Wilkinson's catalyst,⁴⁵ inorganic nanocrystals

such as CdSe^{46,47} and Au,⁴⁸ DNA^{49,50} and various other biological molecules,⁵¹⁻⁵⁴ dendrons,⁵⁵ and polymers.¹⁷ Another strategy for SWNT functionalization employs sidewall reactions such as fluorination with elemental fluorine,⁵⁶ 1,3-dipolar cycloaddition,^{57,58} electrochemical reduction of diazonium salts,⁵⁹ and direct addition of nitrenes, carbenes, and radicals to the unsaturated π -system of the nanotubes.⁶⁰ These side-wall functionalization strategies have been used to result in much higher degree of functionalization than previous approaches allowing chemists to control the properties of these nano-scale materials.

Additionally, a number of recent reports have concentrated on supramolecular functionalization of SWNTs, especially with polymeric structures. The aromatic sidewalls of nanotubes provide the possibility for π -stacking interactions with conjugated polymers⁶¹⁻⁶⁶ as well as polycyclic aromatic hydrocarbons. The use of substituted pyrene molecules for surface attachment of a number of functionalities has also been implemented, where the appended structure has been used to attach proteins,⁶⁷ polymerization initiators,⁶⁸ or aqueous solubilizing groups⁶⁹ in a non-covalent fashion.

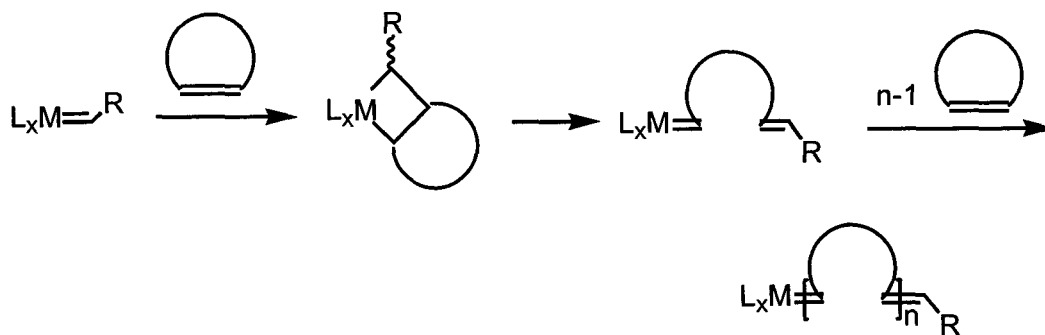
Among all of these chemical modification methods, it has been identified that one of the most promising approaches is the covalent functionalization of carbon nanotubes with polymers.¹⁷ A number of reports have demonstrated the feasibility of attaching amine- and alcohol-functionalized polymeric structures to the surface of SWNTs through amidation and esterification with the carboxylic acid moieties at the ends and defect sites of shortened SWNTs. Using this

“grafting to” approach, SWNT conjugates with various polymers, including poly(ethylene imine),⁷⁰ poly(styrene),⁷¹ poly(ethylene oxide),⁷² poly(vinyl carbazole),⁷³ and poly(vinyl alcohol)⁷⁴ have been prepared. An alternative method that has recently been exploited by our group involves a “grafting from” approach that requires the attachment of polymerization initiators to the nanotubes followed by reaction with appropriate monomers.¹⁸ Since this strategy involves the reaction of nanotubes with small molecules (initiators and monomers, rather than full-length polymers), loss of reactivity due to steric crowding on the nanotube surface is not an issue, and should result in higher grafting density. Additionally, this approach benefits from its modular nature, where the preparation of a single initiator-functionalized nanotube sample can be used for the polymerization of a wide variety of monomers.

1.3 Ring-Opening Metathesis Polymerization (ROMP)

ROMP has attracted significant attention due to its versatility, effectiveness, and functional group tolerance, allowing for a variety of monomers bearing polar, apolar, and charged functional groups to be successfully polymerized.⁷⁵ Scheme 1 shows the process of ROMP in which L_x denotes a generalized ligand coordination sphere. If the cyclic olefin is highly strained such as norbornene, then the reaction is essentially irreversible. It has recently been shown that extremely narrow polydispersities and excellent control over polymer molecular weight and architecture can be achieved if appropriate ligands are utilized, where

high ligand dissociation rates result in rapid initiation of polymerization.^{76,77} All of these factors have made ROMP a useful methodology for the functionalization of surfaces such as Si and SiO₂.^{78,79}



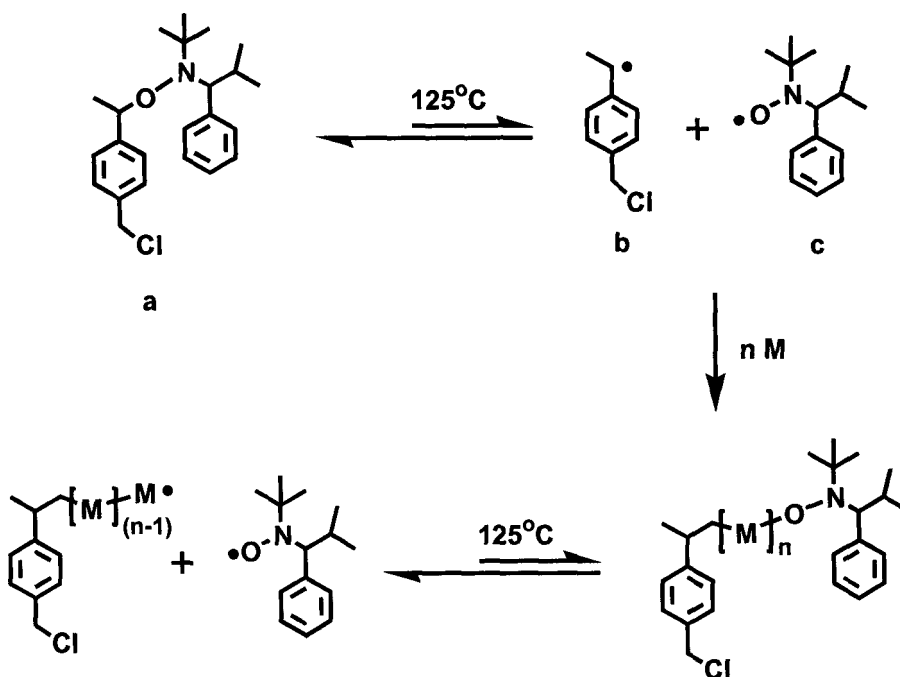
Scheme 1. General mechanism of ROMP.

In fact, successful ROMP from the surface of SWNTs, where the ruthenium alkylidene catalysts were physisorbed on the nanotube surface using pyrene molecules as anchors has already been demonstrated.¹⁸ Although this strategy resulted in successful polymerization and the production of polymer-coated SWNTs, it was shown that high molecular weight polymers tended to desorb from the nanotube surface, as evidenced by a decrease in the nanotube coating thickness when the polymerization time exceeded 5-10 min.⁸⁰

1.4 Stable Free Radical Polymerization (SFRP)

In a typical SFRP process nitroxides such as 2,2,5,5-tetramethyl-3-(1-phenylethoxy)-4-chloromethyl-phenyl-3-azahexane,⁸¹ compound **a**, thermally

decompose (Scheme 2) at 125°C to form carbon-centered free radicals (initiating radicals **b**) and oxygen-centered free radicals (alkoxyamine derivatives **c**). The oxygen-centered free radicals are essentially stable and will not participate in the polymerization, thus acting as radical traps.



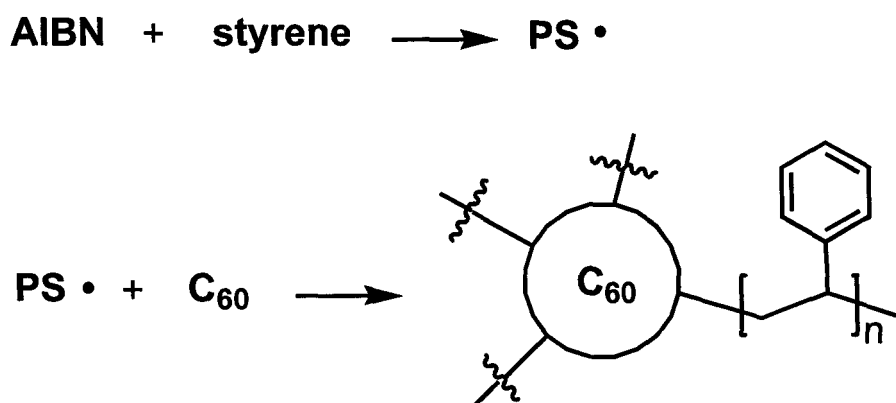
Scheme 2. General mechanism for 2,2,5,5-tetramethyl-3-(1-phenylethoxy)-4-chloromethyl-phenyl-3-azahexane **1** initiated SFRP.

Some additives, such as acetic anhydride and stable free nitroxide radicals (the radical to which the corresponding initiator will thermally decompose) are normally used to obtain a faster polymerization rate and narrower polydispersity.^{82,83} The family of nitroxides⁸⁴ permits the polymerization of a wide variety of monomers: acrylates, acrylamides, 1,3-dienes and acrylonitrile.

However, to date, styrenics are still the easiest monomer family to be polymerized under SFRP in a living manner.

1.5 Radical Coupling Chemistry

Radical coupling chemistry was initially utilized for chemical functionalization of fullerenes.⁸⁵ During the typical free radical polymerization with the presence of fullerenes, the propagating chain radicals can react with the double bonds of the fullerene (Scheme 3). There is no chemical control in this process. Thus the fullerene structure is not well-defined and cross linked materials are usually obtained.



Scheme 3. Functionalization of fullerenes with polymer via free radical polymerization.

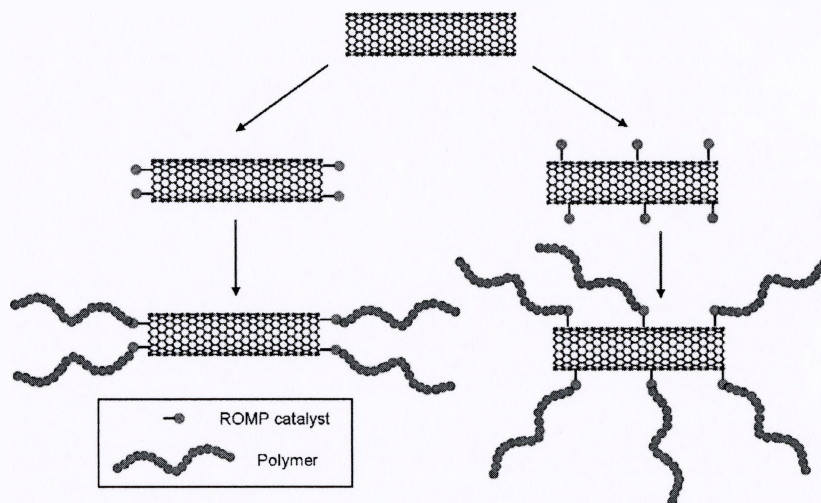
Recently it has been shown that radical coupling chemistry also could be applied to polymer functionalization of carbon nanotubes. Shaffer and Koziol

demonstrated that polystyrene molecules were attached to the surface of oxidized multi-wall carbon nanotubes using an *in-situ* radical polymerization reaction.⁸⁶ Another similar work was carried out by Resasco and co-workers in which SWNT-filled polystyrene and styrene-isoprene composites were prepared by miniemulsion polymerization.⁸⁷ Both of these approaches showed a high polymer grafting efficiency and high solubility of polymer-nanotube composites in toluene. However, the molecular weight of attached polymers was not controlled due to the free radical polymerization process.

Chapter 2 Objectives

2.1 Polymer Functionalization of SWNTs via ROMP

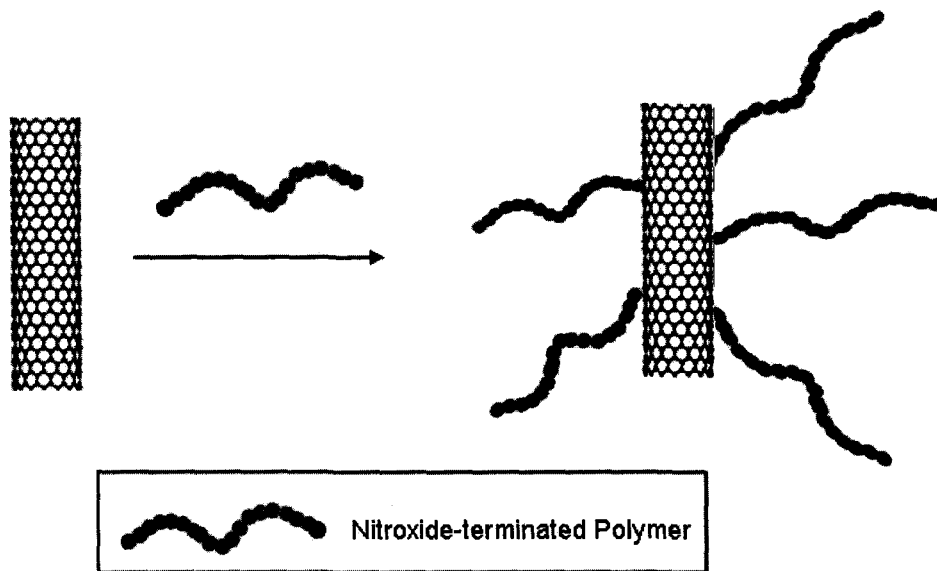
In order to take full advantage of the promising ROMP, shortened SWNTs were covalently functionalized via a “grafting from” approach as an alternative to the supramolecular polymer functionalization that has been mentioned previously.⁶¹⁻⁶⁹ Scheme 4 illustrates the “grafting from” approach utilized in this work in which shortened SWNTs were covalently functionalized with ROMP catalysts to their ends and side-walls respectively. This was followed by their subsequent utilization in the controlled polymerization of norbornene monomers to produce polymers from the nanotube surface. We demonstrate that it is possible to graft high molecular weight polymers to the nanotube surface by this approach, allowing for the modification of nanotube properties such as solubility.



Scheme 4. “Grafting from” approach using ROMP.

2.2 Functionalization of SWNTs via Radical Coupling Chemistry

In an attempt to obtain well-defined polymer-SWNTs nanostructure via an easy method, attachment of well-controlled polymers to the surface of SWNTs was investigated. In this project homo-polymers and diblock copolymers prepared by SFRP, which have well controlled molecular weights and polydispersities, were covalently attached to SWNTs using the efficient radical coupling reaction, with the resulting well-defined polymer-nanotube conjugates exhibiting high solubility in various organic solvents. Furthermore, after chemical modification the diblock copolymer functionalized SWNTs can form aggregates when dissolved in specific solvent systems.



Scheme 5. "Grafting to" approach using radical coupling chemistry.

Chapter 3 Functionalization of SWNTs using ROMP

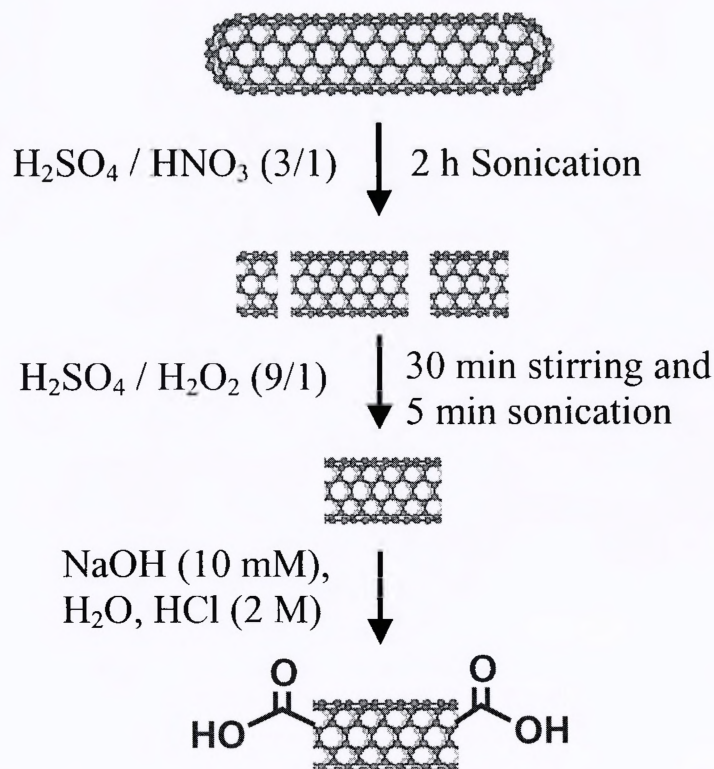
3.1 Overview

Single-walled carbon nanotubes were oxidatively shortened and functionalized with ruthenium-based olefin metathesis catalysts. These catalyst-functionalized nanotubes were shown to be effective in the ring-opening metathesis polymerization of norbornene, resulting in rapid polymerization from the catalyst sites on the nanotube. It was found that high polymer molecular weights could be reached, and the molecular weight increased linearly with polymerization time. The resulting polynorbornene-functionalized nanotubes were found to exhibit solubility in organic solvents, while the starting materials and catalyst-functionalized nanotubes were completely insoluble. The polymerized materials were characterized by NMR, IR, DSC, AFM and TEM.

3.1.1 Shortening and Purification of SWNTs

The starting pristine single-walled carbon nanotubes, which were purchased from Carbon Nanotechnologies Inc., are approximately 1.5 to 2 μm in length, and 1 to 1.5 nm in diameter. Considering our primary goal, which is to make soluble polymer carbon nanotube composites, we assumed that the smaller or shorter structure would have higher solubility. Thus the pristine nanotubes

were shortened following a procedure published by Richard E. Smalley¹⁵ and modified by Zhaoling Yao.¹⁸



Scheme 6. Shortening and purification of SWNTs.

As described in Scheme 6, after sonication in $\text{H}_2\text{SO}_4/\text{HNO}_3$ for 2 h, carbon nanotubes were cut at defect sites followed by washing with hydrogen peroxide and sodium hydroxide solution to remove any impurities and small particles. At the end of this process the length of nanotubes was reduced to an average of approximately 330 nm. Figure 2(A) shows an AFM image of pristine carbon

nanotubes whose lengths are in range of microns. Figure 2(B) shows some much shorter nanotubes or bundles after the shortening procedure.

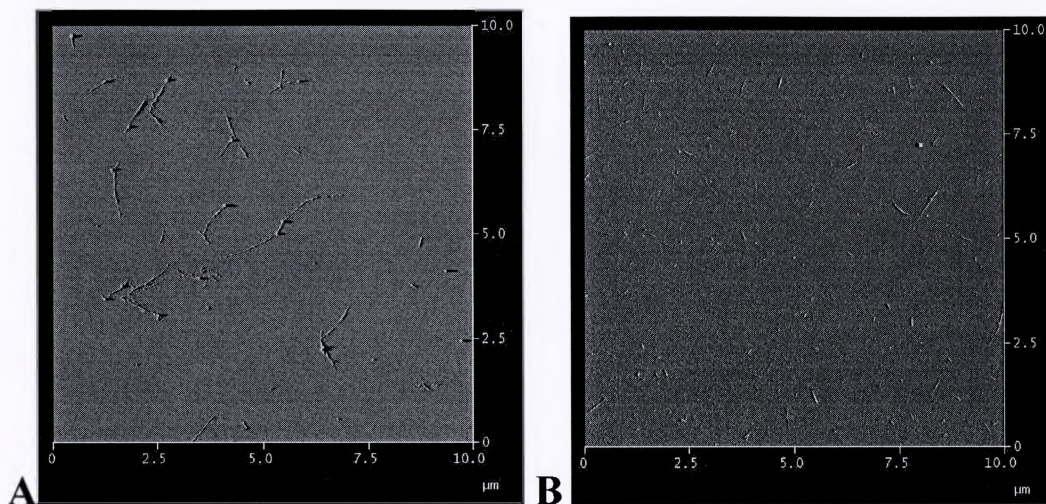


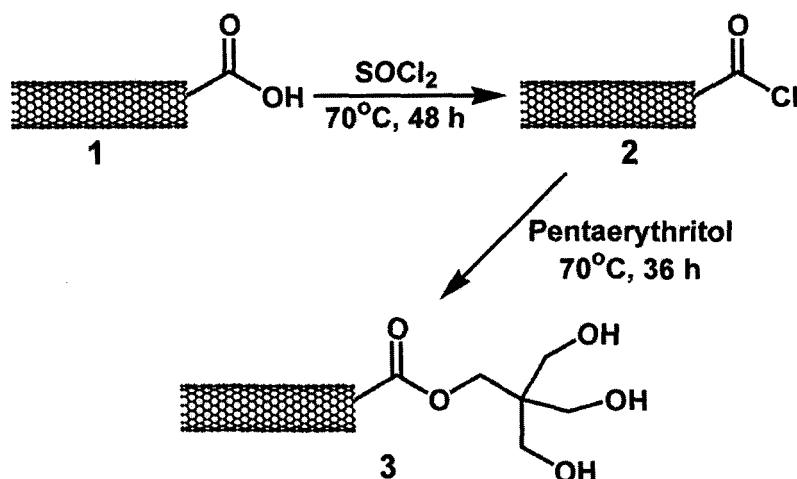
Figure 2. AFM images of (A) Pristine SWNTs, and (B) shortened SWNTs.

The product of this procedure was characterized by IR spectroscopy. The IR spectrum of the shortened nanotubes (Figure 3(A)) depicts the expected C=O stretch at 1748 cm^{-1} corresponding to the carboxylic acid groups introduced as a result of the shortening process. The large IR band observed at 3400 cm^{-1} and the weak one at 1632 cm^{-1} are attributed to the asymmetric bending and scissoring vibrations, respectively, due to trace amounts of water present in the KBr pellet used for the measurement,¹⁸ which could not be removed even with extensive drying of the KBr at elevated temperatures and prolonged purging of the instrument with a stream of nitrogen gas.

3.1.2 Synthesis and Characterization of End Polynorbornene-Functionalized SWNTs

The shortening procedure resulted in carboxylic acid-functionalized nanotubes. These acid groups are mainly located at the two open ends of carbon nanotubes. Additionally there are some defect sites on the side-wall which can also contain acid groups. When functionalization of these SWNTs starts at the acid groups, it can be expected that most polymer chains will grow from the nanotube ends, while some others will grow from defect sites on the side-wall. A significant limitation to this approach is the actual number of acid group per nanotube that are available for functionalization. Considering that HiPco SWNTs have a diameter of 1.0 to 1.5 nm, one nanotube can have, at most, about 100 acid groups on its two ends. After shortening, the nanotubes still have an average length of 330 nm. Thus each carbon nanotube can only contain 0.23 % (by weight) of acid groups. Considering this low functional group concentration, it is clearly difficult to attach catalysts to the nanotubes directly. We concerned that the simplest way to solve this problem is to increase the functional group concentration, thereby increasing the possibility of achieving the desired reaction.

In order to realize this goal, the acid groups were firstly converted to acid-chlorides using thionyl chloride (Scheme 7) and were then treated with pentaerythritol, resulting in the introduction of three primary alcohol functionalities for every reacted acid group of the nanotube. The end triol-functionalized nanotubes (**3**) were then treated with the acid-chloride derivative of

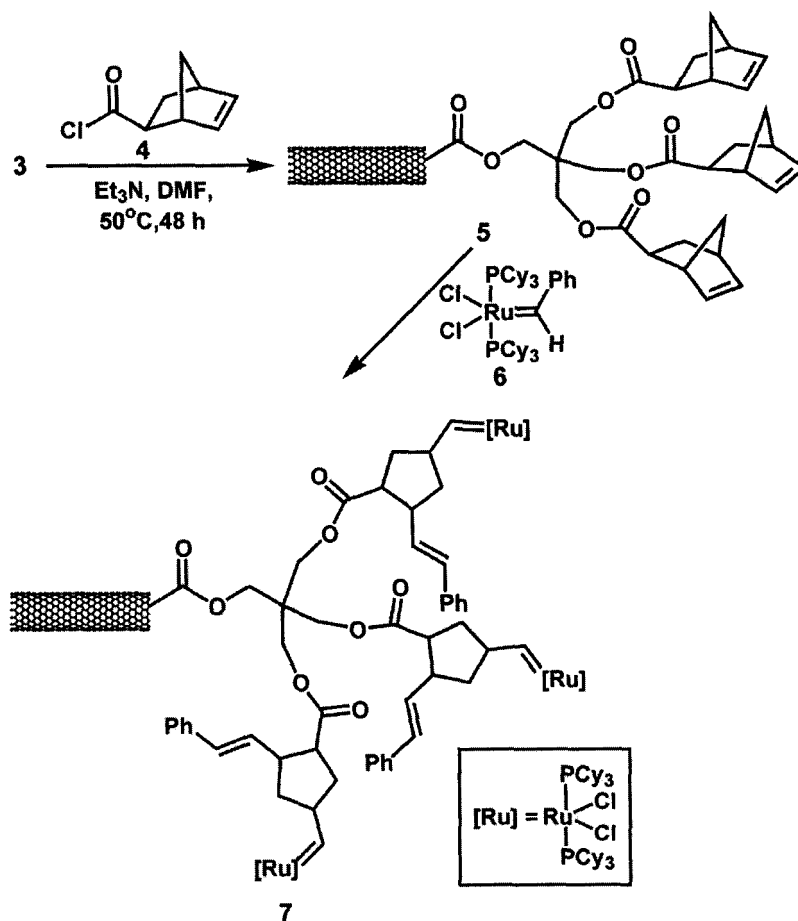


Scheme 7. Synthesis of end triol-functionalized nanotubes (**3**).

5-norbornene-2-carboxylic acid (**4**) to produce the end norbornene-functionalized nanotubes (**5**) which could subsequently be reacted with benzylidene-bis(tricyclohexylphosphine)dichlororuthenium (1st generation Grubbs catalyst, **6**), resulting in the formation of end catalyst-functionalized nanotubes, **7** (Scheme 8). This product was isolated by filtration through a 200 nm-pore diameter Teflon membrane, followed by extensive washing with methanol, dichloromethane, and hexanes to remove any unreacted catalyst. The isolated nanotubes (**7**) can be considered as nanotube-based macroinitiators for ROMP.

Due to the insolubility of the products formed in each of these synthetic steps, their characterization was limited to infrared (IR) spectroscopy. Figure 3 illustrates the IR spectra for the shortened, but unfunctionalized, SWNTs (A) as

well as the end triol-functionalized (B), the norbornene-functionalized (C), and end catalyst-functionalized (D) structures.



Scheme 8. Synthesis of end catalyst-functionalized nanotubes (7).

In Figure 3(B), the appearance of the C-H stretching frequencies at 2875 and 2933 cm⁻¹ clearly indicates the added methylene groups in the triol structure. Furthermore, the asymmetric bending and scissoring vibrations at 3400 cm⁻¹ and 1632 cm⁻¹ respectively, which were due to trace amounts of water present in the

KBr pellet, increased a lot relative to the carbonyl stretch at 1756 cm^{-1} . These increases correspond to the added of hydroxyl groups from **1** to **3**. In Figure 3(C), the carbonyl stretch at 1737 cm^{-1} is clearly indicative of the ester bond formation between the norbornene and the alcohol of the SWNTs in compound **5**. In addition, the large scale increase of the C-H stretching frequencies at 2883 and 2968 cm^{-1} correspond to the added alkyl groups in the transformation from **3** to **5**. Spectroscopic evidence for the conversion of **5** to **7** is more subtle, but can be gathered from an increase in the intensity of the C=C stretch at 1660 cm^{-1} relative to the carbonyl stretch at 1741 cm^{-1} . However, the definitive evidence for the preparation of the SWNT macroinitiator **7** was derived from its ability to promote ROMP. Addition of norbornene to a suspension of **7** in degassed chloroform or heptane resulted in a rapid polymerization from the surface of the nanotubes (Scheme 9). Typical polymerization times ranged from 5 to 180 min. The polymerization products were isolated by filtration through a 200 nm pore-diameter Teflon membrane, followed by thorough washing with dichloromethane, THF, and methanol. The IR spectrum of a typical polymerized product (2 h polymerization time) is depicted in Figure 3(E). The significant intensity of the C-H stretches at 2856 and 2926 cm^{-1} is indicative of the increased number of alkyl groups within the product as a result of norbornene polymerization, and is consistent with the IR of polynorbornene itself. It should be noted that any free polymer that may be formed in solution is easily removed by the filtration/washing step of the work-up.

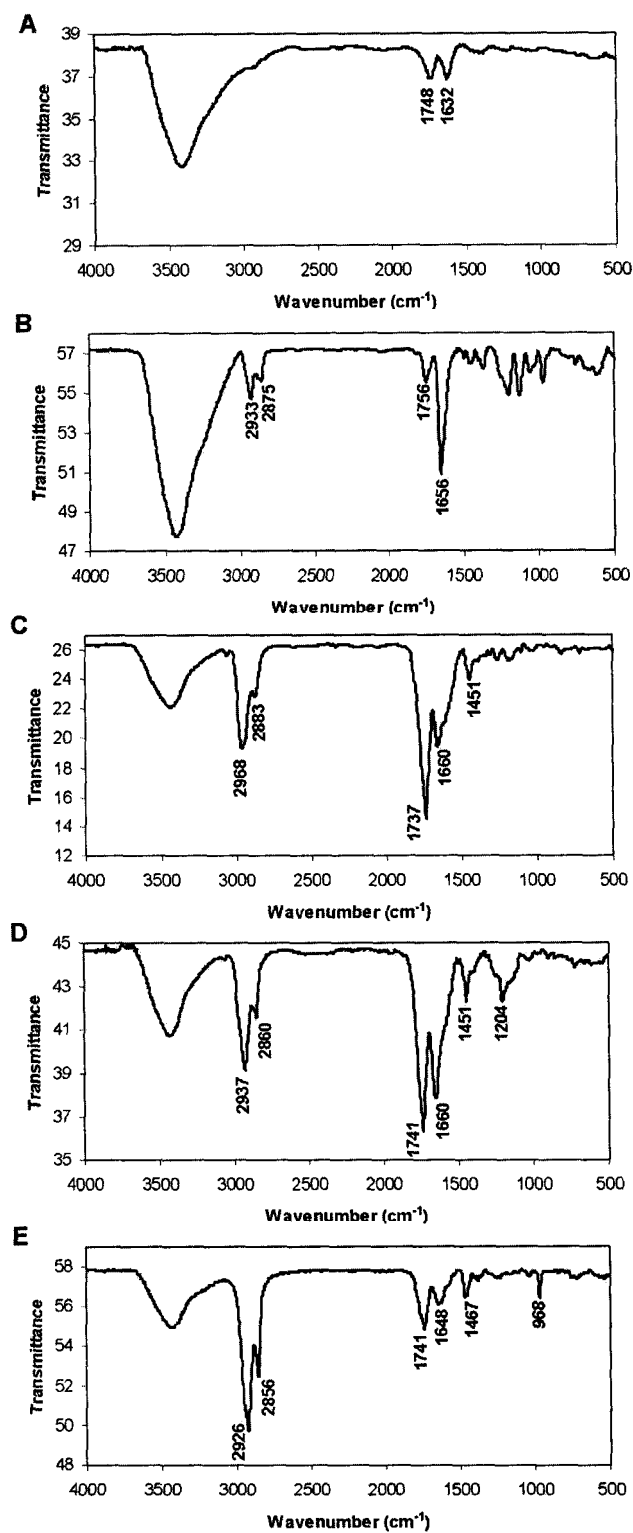
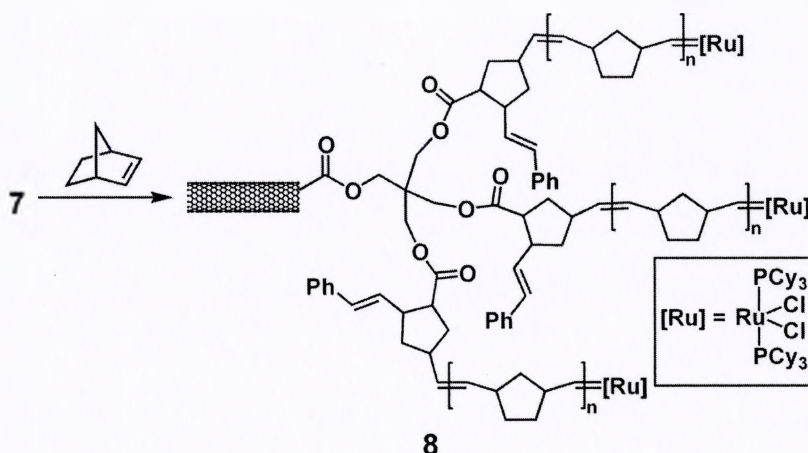


Figure 3. IR spectra of (A) compounds 1, (B) 3, (C) 5, (D) 7, (E) 8.

Control experiments, where the polymerization was carried out in the presence of shortened SWNTs (**1**), but with unattached catalyst **6**, resulted in no detectable attachment of polymers to the nanotubes, as evidenced by the absence of any change in the IR spectrum of the isolated nanotube product from that of the starting material.



Scheme 9. ROMP from SWNTs.

Figure 4 illustrates the Raman spectra of the shortened, unfunctionalized nanotubes (**1**) and the polymerized nanotubes (**8**). In both cases, the characteristic absorptions of the nanotubes are clearly observable at ca. 260 and 1590 cm^{-1} , corresponding to the radial breathing modes (RBM) and the tangential G band, respectively.⁸⁸ In addition, the broad disorder band at 1300 cm^{-1} indicates the presence of sp^3 hybridized C atoms, which are known to occur at defect sites in the nanotube structure.⁵⁹ The strong similarity between the two Raman spectra

indicates that the functionalization and polymerization processes did not significantly alter the nanotube structure.

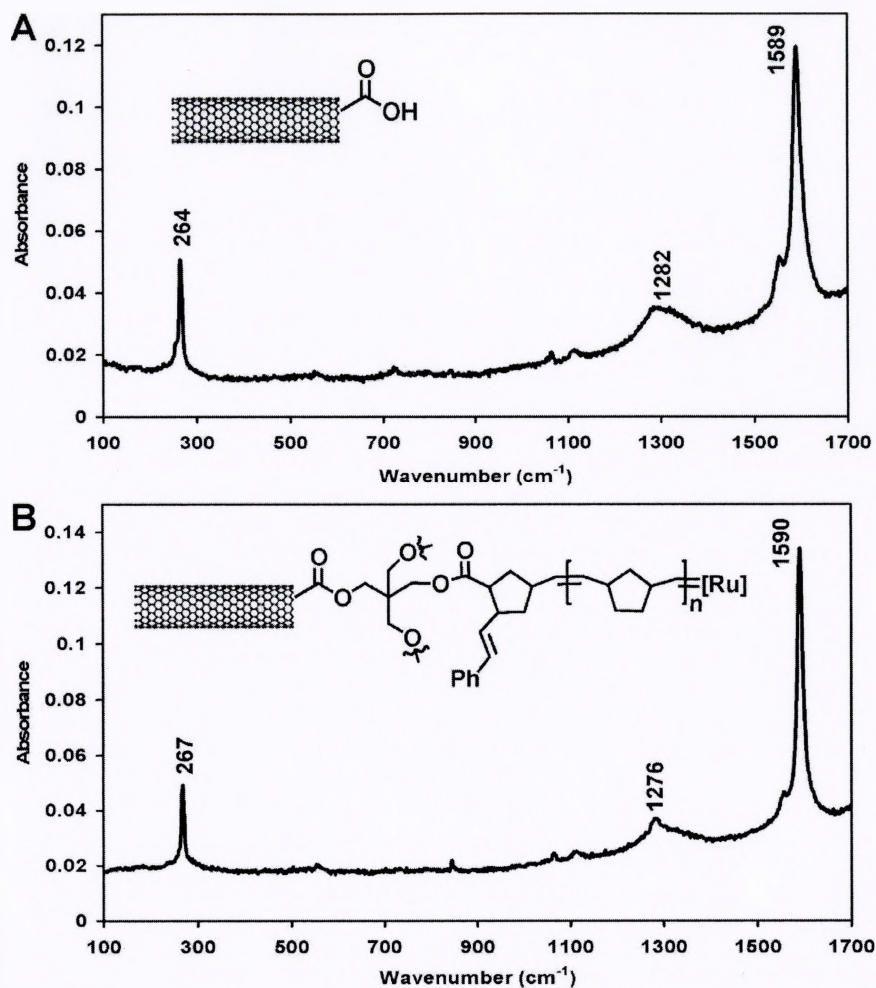


Figure 4. Raman spectra of (A) shortened nanotubes, and (B) end polynorbornene-functionalized nanotubes.

It was found that the solubility of the polymerized nanotubes was influenced by the appended polymers. Prior to the polymerization step, the catalyst-functionalized nanotubes were completely insoluble in all organic

solvents. However, after polymerization, the nanotubes became slightly soluble in THF, chloroform, and dichloromethane (Figure 5).

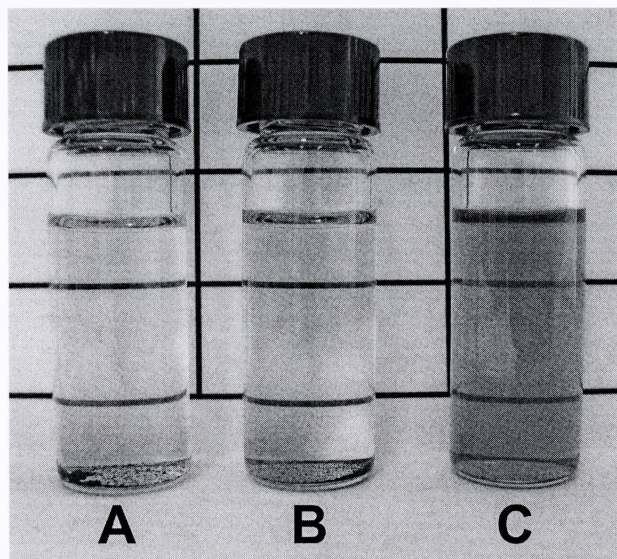


Figure 5. Samples of (A) shortened, unfunctionalized nanotubes **1**, (B) end catalyst-functionalized nanotubes **7**, and (C) polymerized nanotubes **8** in THF.

In an attempt to prove that the solubility of the polymerized nanotubes is really attributed to covalently attached polynorbornene instead of noncovalent interaction between SWNTs and polynorbornene, a control experiment was carried out in which a typical ROMP of norbornene was run with the presence of shortened but unfunctionalized nanotubes. When the resulting mixture was put into THF, all SWNTs were completely insoluble and settled down after a few minutes. The clear solution was taken for UV/Vis measurement. The measured spectrum illustrates that there is no broad absorption at the wavelength expected

for SWNTs (Figure 6(A)). In comparison the UV/Vis absorption of end polynorbornene-functionalized nanotubes **8** shows a typical UV/Vis spectrum of SWNTs (Figure 6(B)).

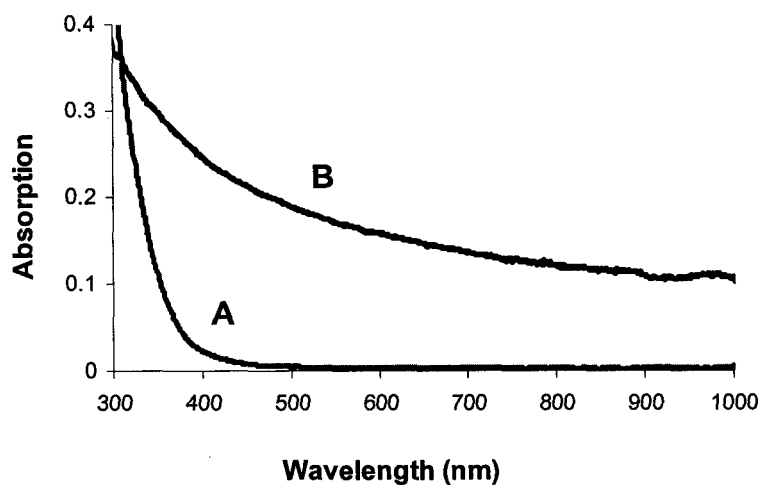


Figure 6. UV/Vis spectra of (A) mixture of polynorbornene and shortened nanotubes, and (B) end polynorbornene-functionalized nanotubes.

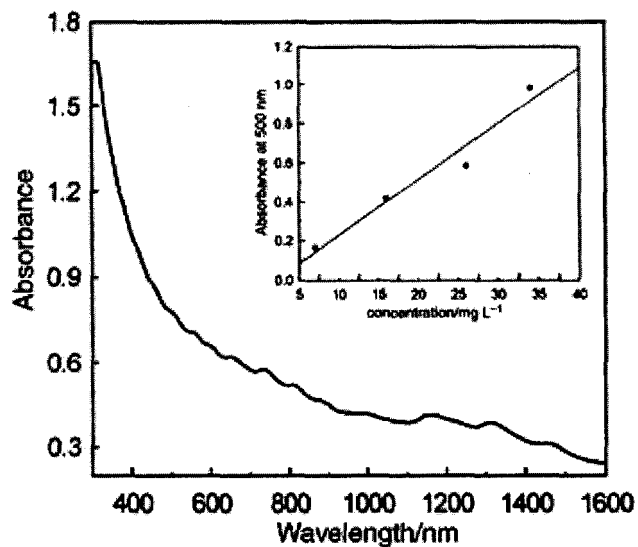


Figure 7. Calibration curve of SWNTs reported by Smalley.⁸⁹

Utilizing the previously published specific extinction coefficient for SWNTs ($\epsilon_{500} = 28.6 \text{ cm}^2/\text{mg}$) (Figure 7),⁸⁹ we were able to estimate the nanotube concentration to be ca. 19 mg/L. Although it is quite low, this level of solubility nevertheless allowed for the use of solution NMR in the characterization of the polymer-nanotube composites. Figure 8 depicts the ^1H NMR spectra of polynorbornene and the polymerized nanotubes **8**. The two spectra are nearly identical, indicating that norbornene monomers were, indeed, polymerized with the use of the nanotube macroinitiators. The ^{13}C NMR spectra of polynorbornene and the polymerized nanotubes **8** (Figure 9) also prove that polynorbornene was grown from the nanotube macroinitiator.

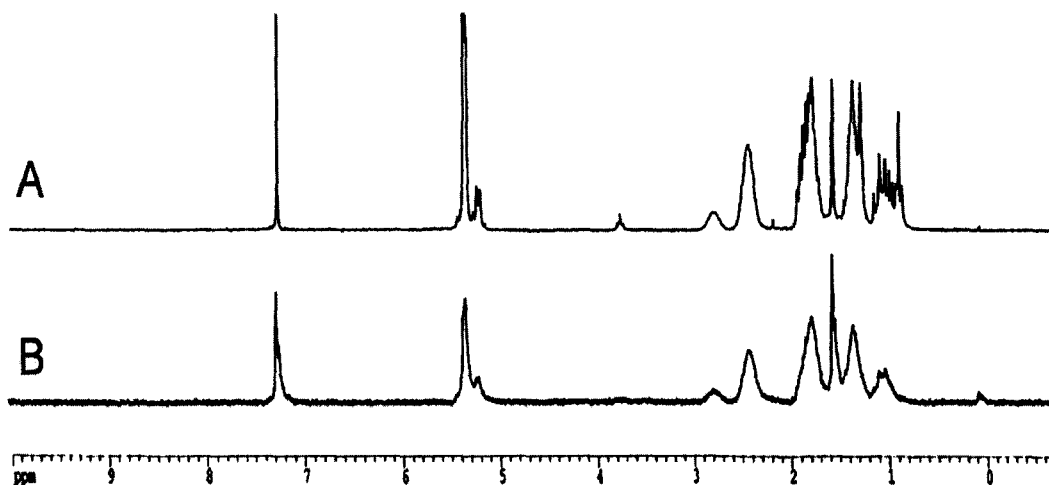


Figure 8. ^1H NMR spectra of (A) polynorbornene, and (B) polynorbornene-functionalized nanotubes.

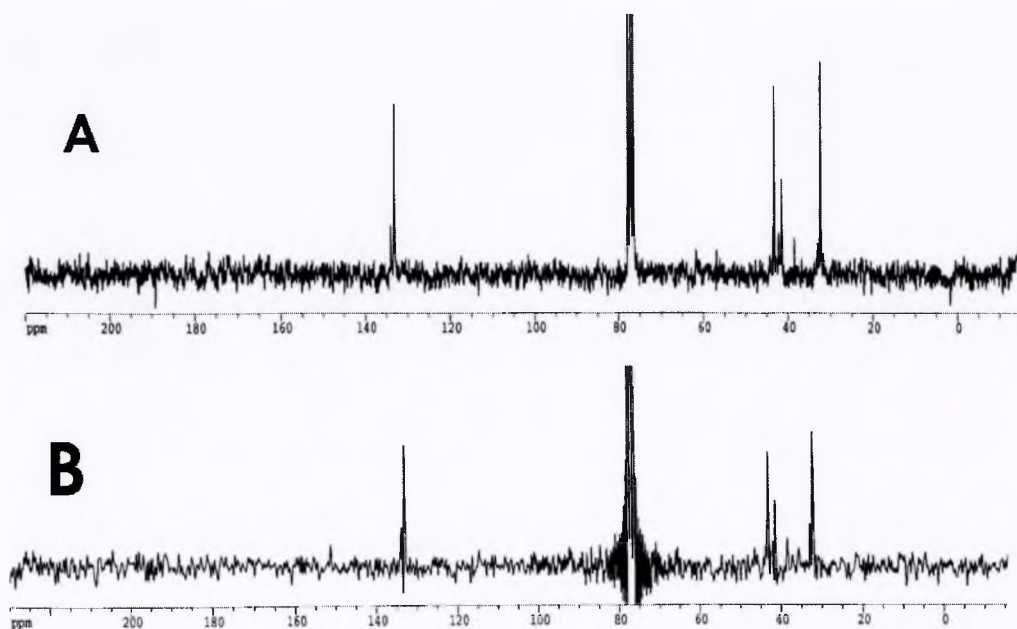


Figure 9. ^{13}C NMR spectra of (A) polynorbornene and (B) polynorbornene-functionalized nanotubes.

To further explore the topological properties of the hybrid materials, atomic force microscopy (AFM) was utilized. Sample preparation involved spin-coating several drops of the nanotube solution onto a mica substrate. Prior to polymerization, the end initiator-functionalized nanotubes were indistinguishable from typical unfunctionalized structures, associating in small bundles with diameters in the range of 1-3.5 nm (Figure 10(A)). However, after polymerization, larger features were observable, corresponding to SWNTs that are surrounded by domains of polymer (Figure 10(B)). In some cases, it was possible to observe larger polymer domains near the ends of the nanotubes, likely because most of the initiators were attached to the carboxylic acid groups mainly located

at the open nanotube ends (Figure 10(C)). Other structures seemed to have polymer regions evenly distributed along the entire length of the nanotube, likely due to polymer wrapping, or the attachment of polymerization catalysts at defect sites along the side-walls of the nanotubes (Figure 10(D)). Height profiles for the polymerized structures indicated that the height of the features increased to 8-15 nm as a result of the appended polymer structures (see the profile traces below images C and D of Figure 10). However, it is not possible to ascertain whether the observed features contain individual nanotubes or bundles of tubes.

Further characterization of the polymerized nanotubes was done using transmission electron microscopy (TEM), as depicted in Figure 11. Again, solutions of **8** in THF were drop-cast onto a holey carbon-coated copper grid and allowed to air-dry. Low magnification TEM images highlighted the presence of sheets and fibers of amorphous carbon in which, upon close inspection, it was possible to discern the presence of SWNTs. It appeared as though the nanotubes were embedded within a matrix of amorphous carbon, which corresponds to the polymer coating on the SWNTs. In some areas, it was also possible to observe portions of single nanotubes spanning the gap between two regions of polymer (Figure 11, inset).

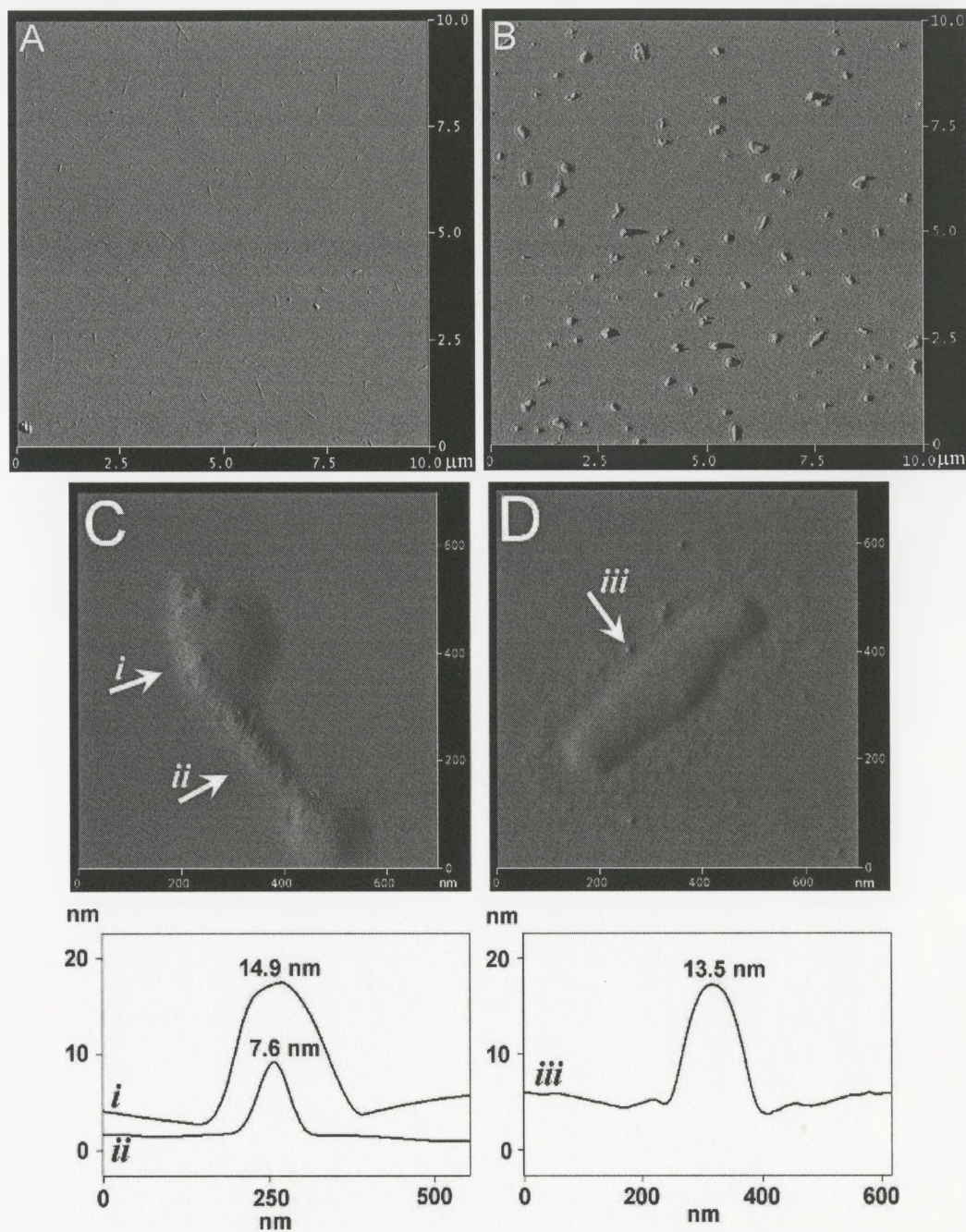


Figure 10. AFM images of nanotubes before (A) and after (B) polymerization. Two close-ups of individual structures, (C) and (D), illustrate that the polymer density can be localized near the ends of the tubes in some cases (C) and along the entire wall of the tubes in others (D). Profile traces at different points along the features are given below the AFM images (C) and (D).

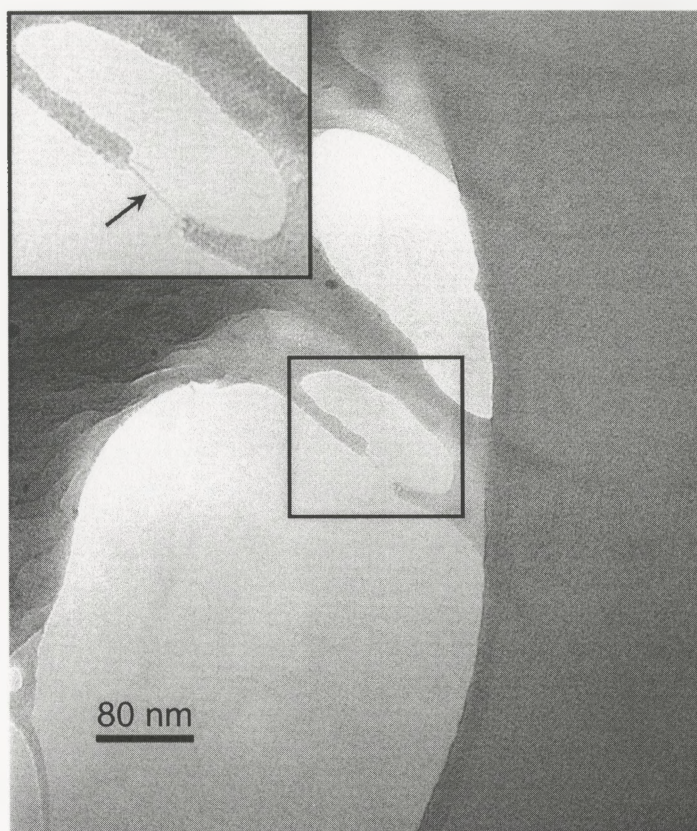
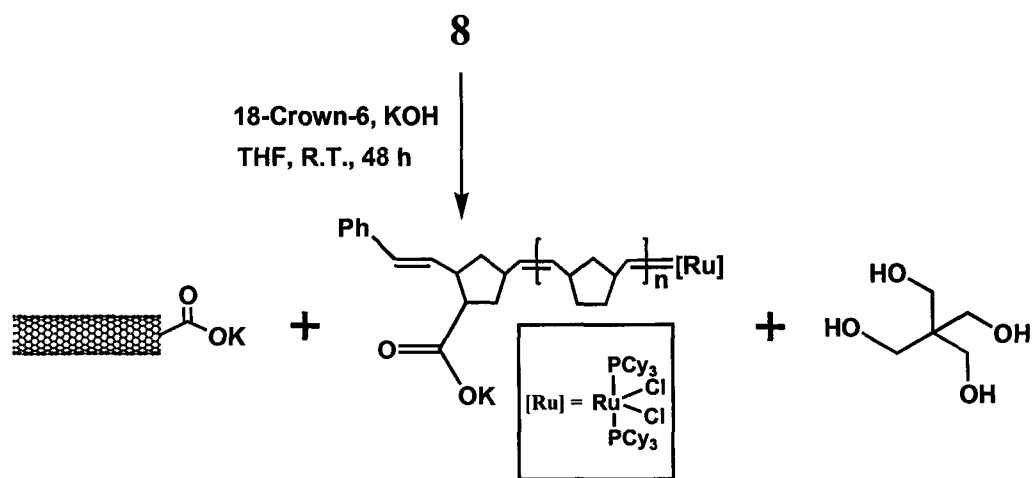


Figure 11. TEM image of end polymer-functionalized nanotubes. The inset is a blow-up of the region within the box, showing a single nanotube bridging the gap between two polymer regions (arrow).

To determine the effect of polymerization time on polymer molecular weight, we analyzed the polymers produced in a series of polymerizations that ranged from 5 min to 180 min in duration. Nanotube bound polymers were cleaved by saponification of the ester linkages with KOH/18-crown-6 in THF for 48 h at room temperature (Scheme 10). The SWNTs were separated from the

cleaved polymer by filtration through a 200 nm pore-diameter Teflon membrane, leaving the pure polymer in the filtrate. Figure 12 shows the ^1H NMR spectra of pure polynorbornene and isolated polynorbornene. They are identical, proving that polynorbornene was successfully cleaved from nanotube composites. Gel permeation chromatography (GPC) analysis of the isolated polymers revealed a linear increase in molecular weight with increasing polymerization time (Figure 13). The polydispersities of the samples were found to remain relatively constant at all polymerization times.



Scheme 10. Defunctionalization of end functionalized polynorbornene-SWNT composites.

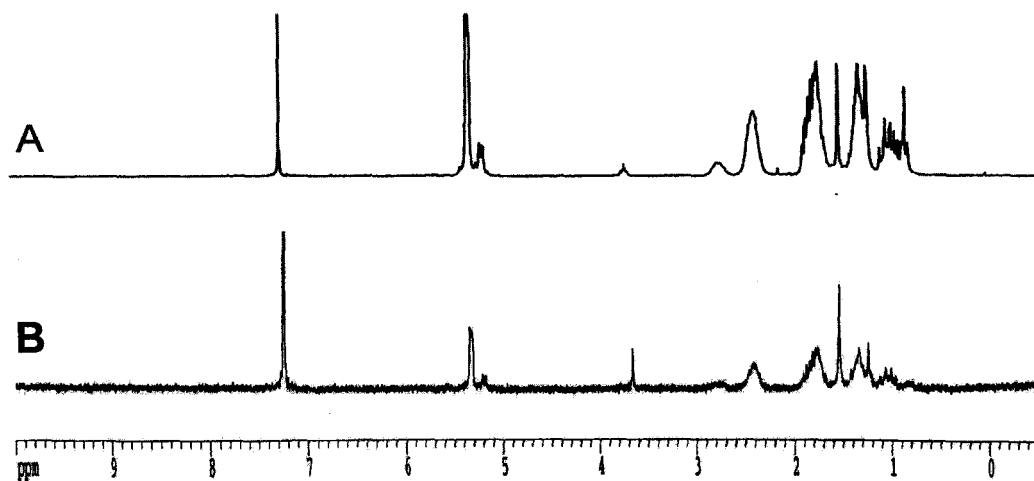
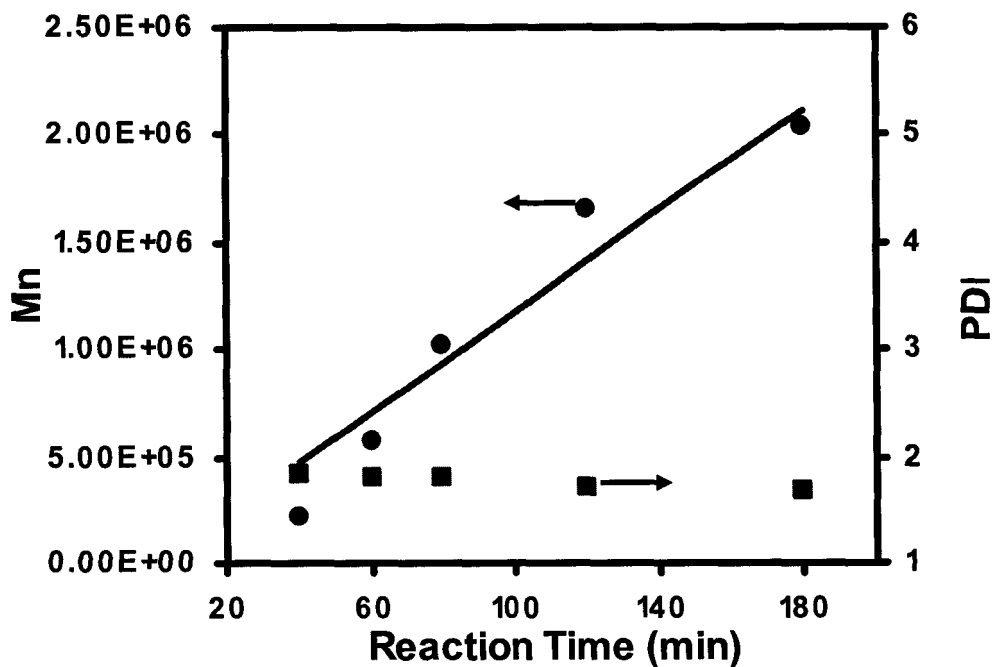


Figure 12. ^1H NMR spectra of (A) polynorbornene and (B) cleaved



polynorbornene.

Figure 13. Plot of the molecular weight and polydispersity of polynorbornene cleaved from the SWNTs as a function of polymerization time.

It was also possible to measure the glass transition temperature of the polynorbornene before and after cleavage from the nanotubes. As shown in Figure 14(A), unfuntionalized carbon nanotubes don't show any glass transition temperature. The nanotube bound polymers were found to exhibit a Tg of 37°C (Figure 14(B)). After cleavage, the Tg was found to decrease to 27°C (Figure 14(C)), which is very similar to previously reported literature values for polynorbornene.⁹⁰ The higher Tg observed for the nanotube-bound polymers is due to their decreased mobility as a result of nanotube attachment, and is consistent with our earlier observations with PMMA-functionalized nanotubes,¹⁸ as well as other literature reports of surface-bound polymers.⁹¹

In order to measure the weight percentage of polymers in the composites thermogravimetric analysis (TGA) was carried out. Figure 15 illustrates the TGA trace of polynorbornene functionalized nanotubes. Attached polynorbornene started to decompose from 400°C and finished at 500°C while carbon nanotubes remained stable up to 900°C. From the mass decrease we calculated that this polynorbornene-functionalized nanotube contained 90% (by weight) of polynorbornene and 10% (by weight) of carbon nanotubes.

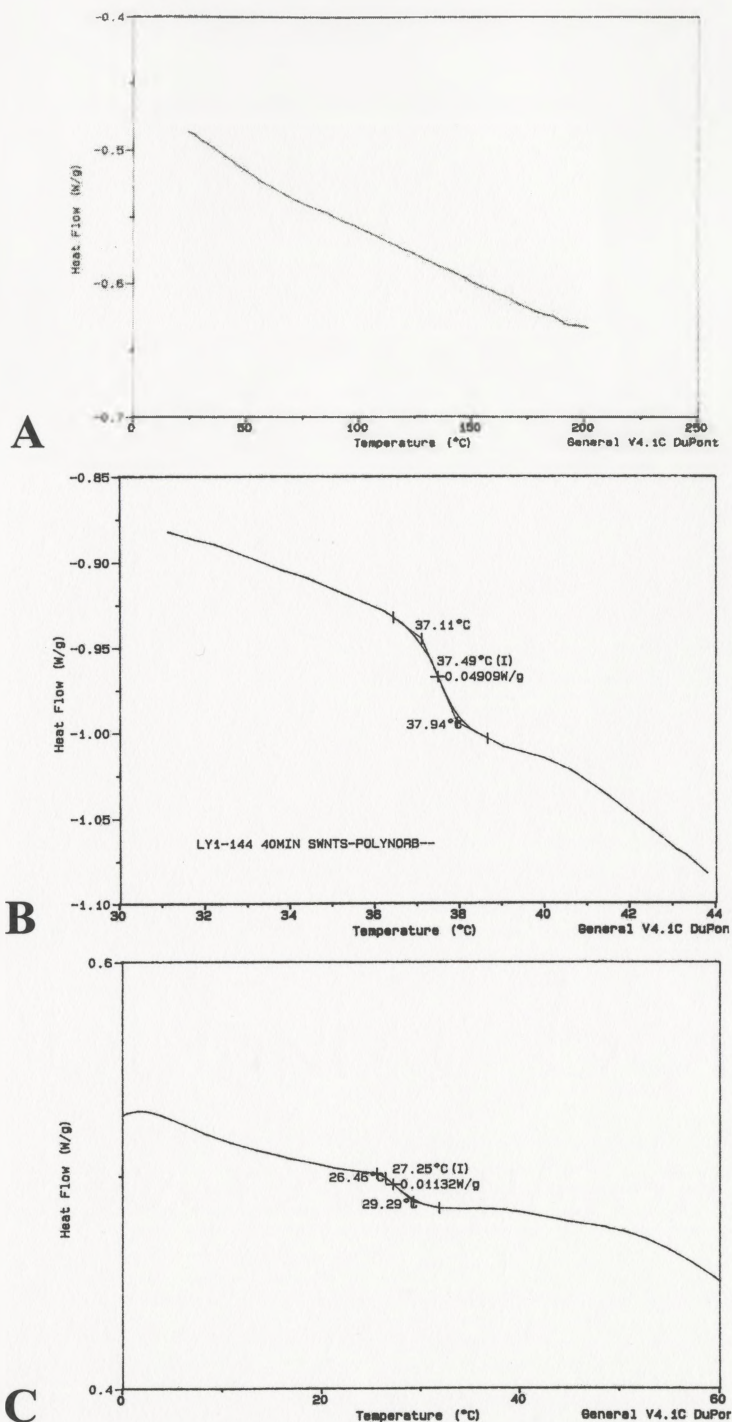


Figure 14. DSC traces of (A) unfunctionalized carbon nanotubes, (B) polynorbornene functionalized nanotubes and (C) cleaved polynorbornene.

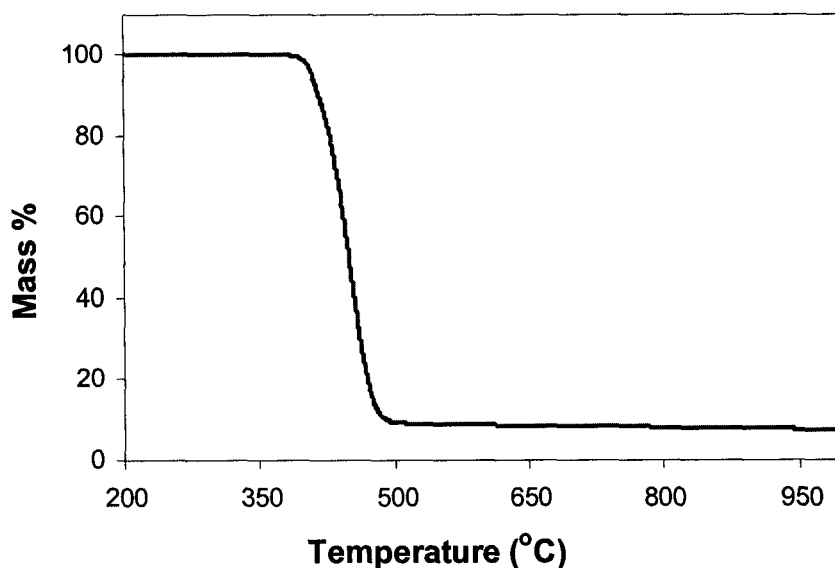
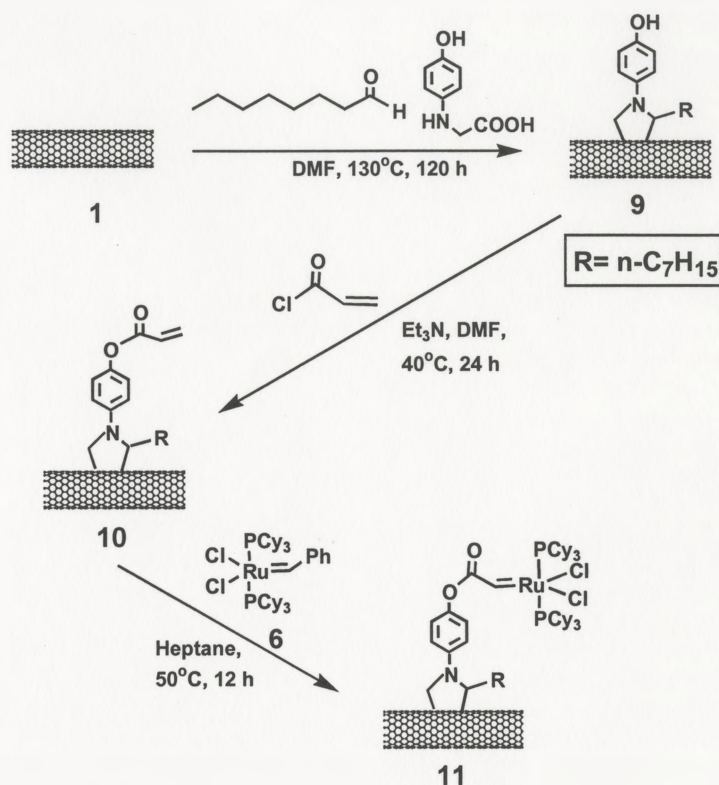


Figure 15. TGA traces of polynorbornene functionalized nanotubes.

3.1.3 Synthesis and Characterization of Side-wall Polynorbornene-Functionalized SWNTs

In order to functionalize carbon nanotubes from side-walls, a 1,3-dipolar cycloaddition^{18,57,58} was adopted to introduce phenol functionalities, followed by an esterification with acryloyl chloride to produce the side-wall norbornene-functionalized nanotubes which can be used to attach Grubbs catalyst, as described above (Scheme 11). Shortened SWNTs were dispersed in DMF to form a suspension followed an addition of 4-hydroxyphenyl glycine and octyl aldehyde. After heating at 130°C for five days it resulted in the incorporation of phenol-functionalized pyrrolidine rings on the side-wall of the SWNTs (9). This

can be proven by the appearance of a clear C-H stretch at ca. 2900 cm^{-1} and an increase in the aromatic C-C stretch at 1634 cm^{-1} in the IR spectrum (Figure 16(B)). The side-wall phenol functionalities could then be treated with acryloyl chloride in DMF at 40°C to introduce vinyl functionalities on the nanotube side-walls (**10**). This functionalization step was again followed by IR spectroscopy to monitor the appearance of a strong C=O stretch (ca. 1740 cm^{-1}) arising from the ester linkages (Figure 16(C)). Then the Grubbs catalyst (**6**) can be attached to nanotubes by reacting with the vinyl groups to make the side-wall functionalized macroinitiator (**11**). This product was also characterized by IR spectroscopy. The large scale increase of the C-H stretching frequencies at 2856 and 2926 cm^{-1} correspond to the added alkyl groups in the transformation from **10** to **11**. There is another increase in the intensity of the C=C stretch at 1662 cm^{-1} relative to the carbonyl stretch at 1767 cm^{-1} . Furthermore, the definitive evidence for the preparation of this side-wall SWNT macroinitiator **11** was derived from its ability to promote ROMP. Similar to the end functionalized macroinitiator, addition of norbornene to a suspension of **11** in degassed chloroform or heptane resulted in a ring-opening metathesis polymerization from the side-walls of the nanotubes (Scheme 12). The polymerization products were isolated by filtration as described above.



Scheme 11. Synthesis of side-wall catalyst functionalized SWNTs (11).

Figure 16(E) illustrates the IR spectrum of a polymerized SWNT sample after 5 min of polymerization, clearly indicating the expected huge increase of C-H stretches at 2871 and 2952 cm^{-1} arising from the nanotube-attached polynorbornene in the sample. The presence of carbon nanotubes in this residue was confirmed by Raman spectroscopy, which revealed their characteristic tangential G-band at ca. 1592 cm^{-1} and radial breathing modes at 267 cm^{-1} (Figure 17). The peak at 1277 cm^{-1} corresponds to the presence of a relatively small amount of sp^3 hybridized carbon atoms, formed as a result of sidewall functionalization (Figure 17).^{59,92}

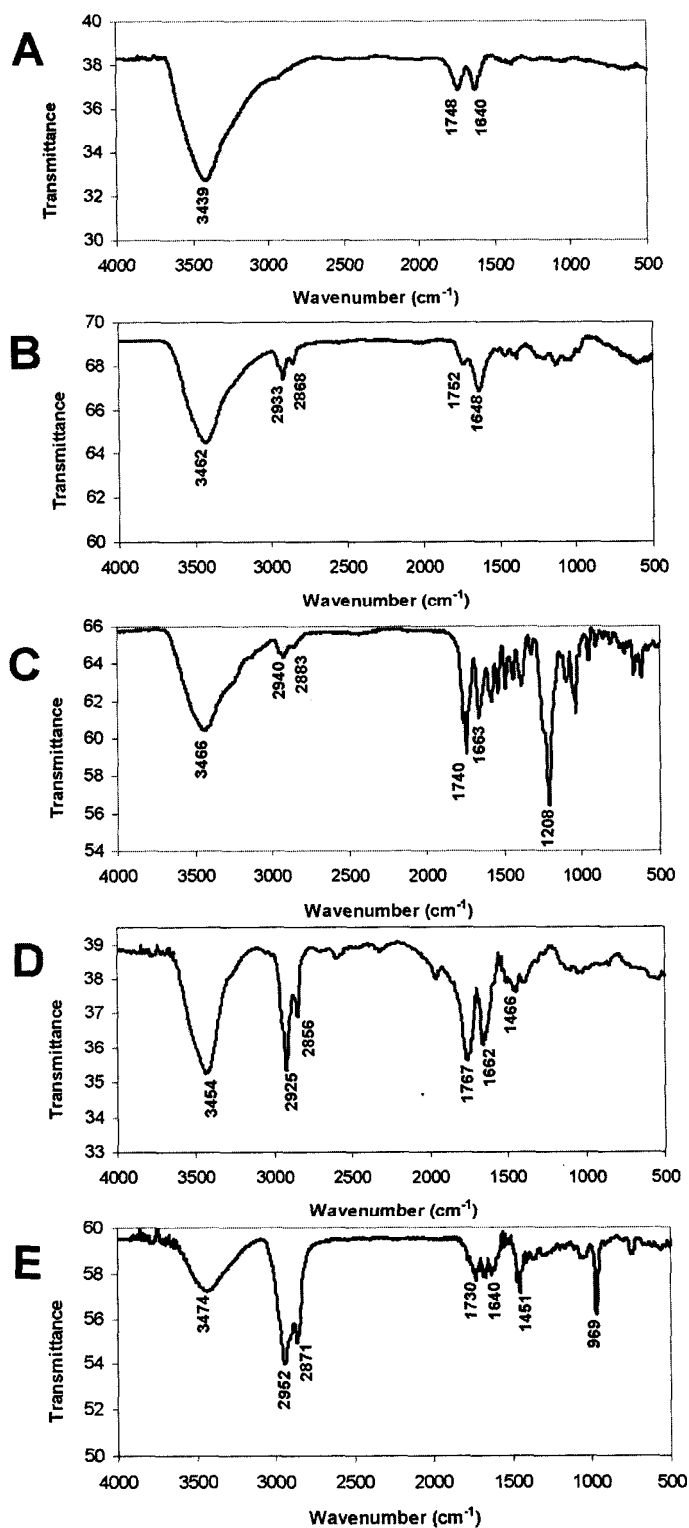
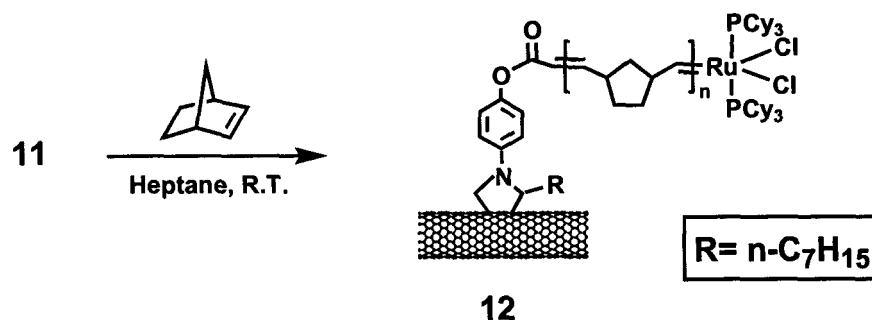


Figure 16. IR spectra of (A) compounds 1, (B) 9, (C) 10, (D) 11, (E) 12.



Scheme 12. ROMP from side-wall of SWNTs.

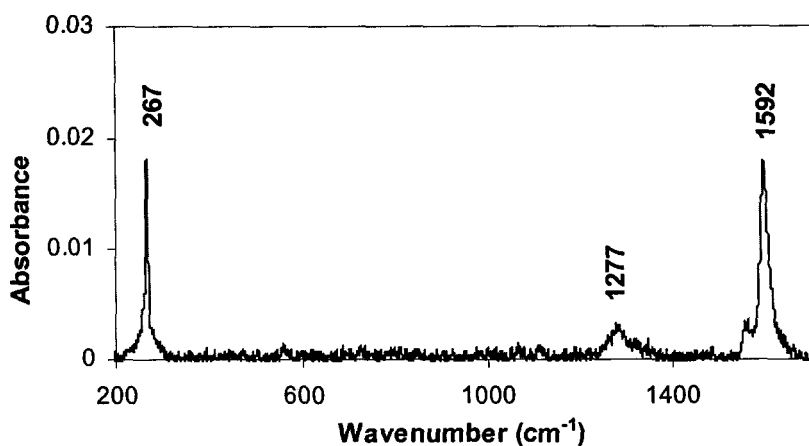


Figure 17. Raman spectrum for the side-wall polynorbornene functionalized SWNTs (12).

AFM was also utilized to characterize the topological properties of the side-wall functionalized nanotubes. The specimen was prepared following the same procedure used for the end polymer-functionalized SWNTs. Figure 18(A) describes a typical amplitude image of side-wall polynorbornene-functionalized nanotubes. It clearly shows that polymer domains surround the entire side-wall of

a single tube or a tube bundle, as would be expected for nanotubes functionalized from their side-walls. Height profiles (Figure 18(B)) for this polymerized structure indicated that the tubes coated with polymer domains have a height range of ca. 8-25 nm, while uncoated areas only have a height about 2 nm, which also matches the height of unfunctionalized nanotubes.

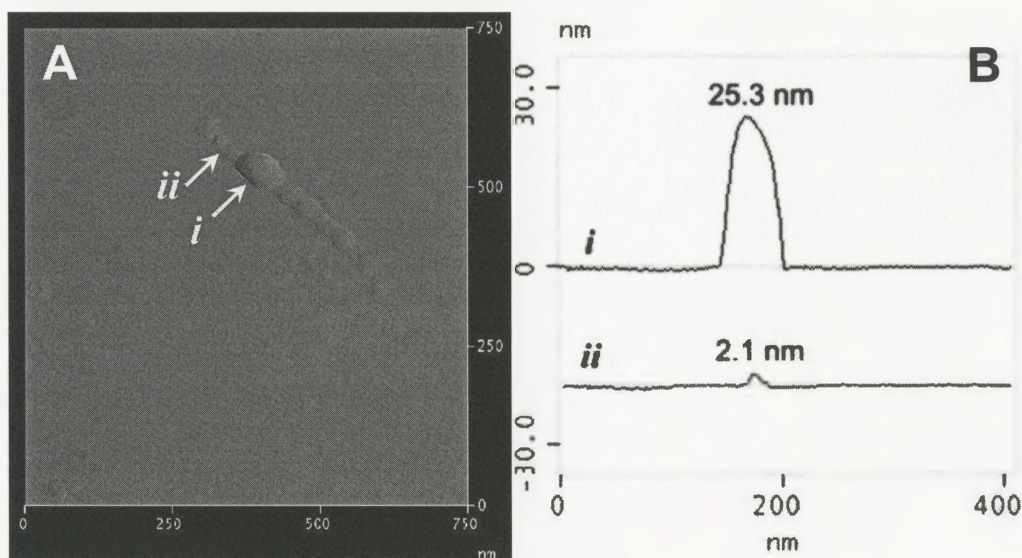


Figure 18. AFM images of (A) side-wall polynorbomene functionalized SWNTs (**12**) and (B) the profile traces at different points along the features are given.

TEM is still the most direct method to observe carbon nanotubes even after polymer functionalization. A TEM specimen was prepared by drop-casting solutions of **12** in THF onto a holey carbon-coated copper grid and allowed to air-dry. Again, the low magnification TEM image (Figure 19) shows the presence of

a polymer film. It is also possible to identify carbon nanotubes when high magnification was used (Figure 19, inset). The arrow points to a couple of

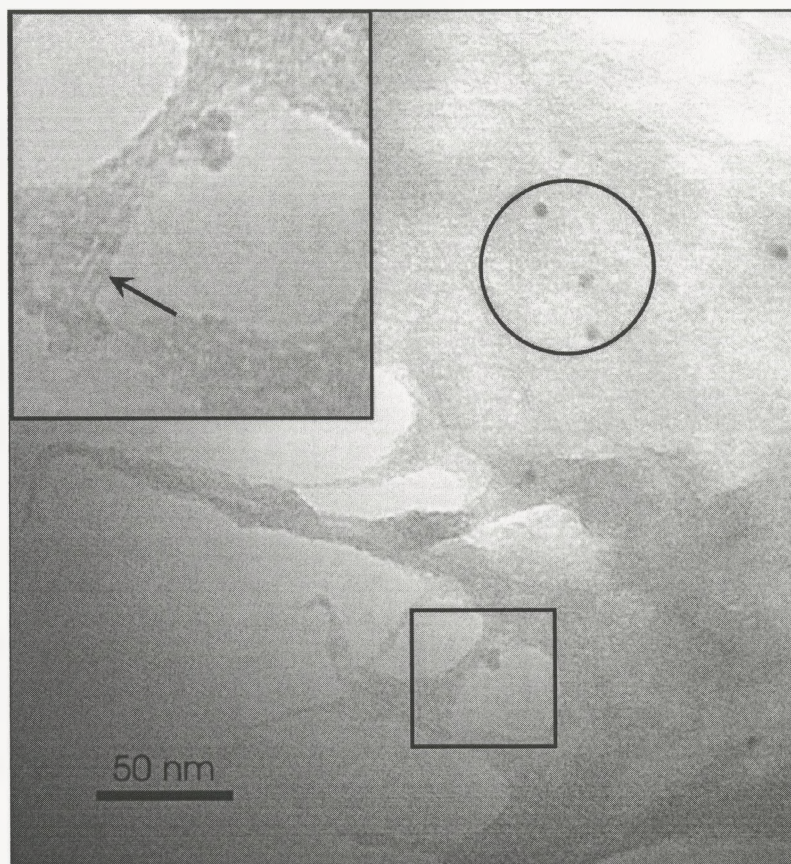


Figure 19. TEM image of side-wall polynorbornene functionalized SWNTs (12). The inset is a blow-up of the region within the box, showing a small single nanotube bundle which was surrounded by polymer (arrow).

single tubes which were mostly coated with polymer domains. Meanwhile there are also some dark particles present in the TEM image, which may correspond to the metal nanoparticles that served as catalyst for nanotube growth.

3.2 Experimental

General. Single-walled carbon nanotubes (SWNTs) were purchased from Carbon Nanotechnologies, Inc. (Houston, TX). N-(4-hydroxyphenyl)glycine was purchased from Aldrich and purified by recrystallization in distilled H₂O. Pentaerythritol, octyl aldehyde, 5-norbornene-2-carboxylic acid, acryloyl chloride, thionyl chloride, 18-crown-6, triethylamine, benzylidene-bis(tricyclohexylphosphine)dichlororuthenium (Grubbs catalyst, 1st generation) and norbornene were all purchased from Aldrich and used without further purification. All other reagents and solvents were purchased from commercial suppliers and used as received. FTIR was performed on a Bio-Rad FTS-40 instrument. All samples were prepared as pellets using spectroscopic grade KBr in a Carver press at 15 000 psi. Laser Raman spectroscopy was performed on a Bruker RFS 100 instrument equipped with a YAG laser and a Ge high-sensitivity detector. Atomic Force Microscopy was done using a Digital Instruments NanoScope IIIa Multimode AFM, with samples prepared by spin casting (4000 rpm) sample solutions or suspensions on freshly cleaved mica substrates. The images were recorded with standard tips in tapping mode at a scan rate of 0.5 Hz. TEM analysis was performed using a Philips CM12 operating at 120 keV. NMR was performed on a Bruker 200 MHz instrument in CDCl₃. Differential scanning calorimetry (DSC) was performed on a TA 2100 Modulated Differential Scanning Calorimeter with a temperature gradient of 15 degrees/min. Thermogravimetric analysis (TGA) was carried out on a NETZSCH STA 409 PC instrument under Ar

with a temperature range from 20°C to 800°C and a temperature gradient of 5 degrees/min. Ultrasonication was done in a Banson Ultrasonics B1510 bath sonicator. Filtration was done through either a 100 nm-pore diameter polycarbonate membrane (Millipore), or a 200 nm-pore diameter Teflon membrane (Millipore). Polymer molecular weight and polydispersity index (PDI) were estimated by gel permeation chromatography (GPC) using a Waters 2695 Separations Module equipped with a Waters 2996 Photodiode Array Detector, a Waters 2414 Refractive Index Detector, a Waters 2475 Multi λ Fluorescence Detector, and four Polymer Labs PLgel individual pore size columns. Polystyrene standards were used for calibration, and tetrahydrofuran (THF) was used as the eluent at a flow rate of 1.0 mL/min. The concentrations of the soluble polymer functionalised SWNTs were calculated from UV/Vis absorption results obtained using a Varian Cary 50 Bio UV-Visible Spectrophotometer.

Shortening and Purification of SWNTs. A 250 mL flask charged with SWNTs (100 mg) and a $\text{H}_2\text{SO}_4/\text{HNO}_3$ (v/v: 3/1) (120 mL) solution was sonicated for 2 h. Then the suspension was diluted in a 1000 mL beaker with distilled water (800 mL). After cooling to room temperature, the dilute solution was filtered through a 100 nm-pore diameter polycarbonate membrane. The black material collected on the membrane was added to a 250 mL flask and stirred with $\text{H}_2\text{SO}_4/\text{H}_2\text{O}_2$ (v/v: 9/1, 50 mL) for 30 min at room temperature. Another 50 mL of $\text{H}_2\text{SO}_4/\text{H}_2\text{O}_2$ (v/v: 9/1) was added and the suspension was sonicated for 5 min. After dilution using distilled water (800 mL) in a 1000 mL beaker, the suspension

was filtered again. The SWNT mat was washed thoroughly using NaOH solution (10 mmol, 250 mL) and distilled water until the pH of the filtrate was 7. Then the nanotubes were washed with an HCl solution (2.0 M, 50 mL) before drying under vacuum overnight. The product was obtained as a black solid (70.0 mg, 70% yield). IR (KBr pellet): $\nu = 1748$ (m), 1632 (m) cm^{-1} .

Synthesis of end triol-functionalized SWNTs (3). Shortened and purified SWNTs (44.0 mg) were added to thionyl chloride (10.0 mL, 137 mmol) in a 25 mL flame dried flask. The suspension was stirred under Ar at 70°C for 48 h to convert the acid groups to acid chlorides. The residual thionyl chloride was evaporated in vacuo. Pentaerythritol (0.5 g, 3.7 mmol) and THF (10 mL) were then added into the flask. The suspension was stirred at 70°C for another 36 h. The reaction mixture was then filtered through a 200 nm-pore diameter Teflon membrane, followed by washing with CH_2Cl_2 (300 mL), THF (100 mL) and methanol (100 mL). The recovered residue was finally dried under vacuum overnight, yielding 50 mg of product. IR (KBr pellet): $\nu = 3442$ (s), 2929 (w), 2871 (w), 1752 (w), 1656 (m) cm^{-1} .

Synthesis of end norbornene-functionalized SWNTs (5). The mixture of 5-norbornene-2-carboxylic acid (3.0 mL, 24.5 mmol) and thionyl chloride (8 mL, 109.7 mmol, 4.5 eq.) in a flame-dried 25 mL flask was stirred at reflux under Ar for 24 h. It was then cooled, evaporated to dryness, and used directly. Triol-functionalized SWNTs (3) (48 mg), were added to the 5-norbornene-2-carboxylic acid chloride along with 10 mL of CH_2Cl_2 , 1 mL of anhydrous DMF, and 1 mL of

triethylamine. The suspension was stirred at 50°C under Ar for 48 h. The product was isolated by filtration through a 200 nm-pore diameter Teflon membrane, followed by washing with methanol (300 mL), THF (100 mL), and CH₂Cl₂ (200 mL). The recovered residue was then dried under vacuum overnight, yielding 53 mg of product. IR (KBr pellet): $\nu = 2968$ (m), 2883 (w), 1737 (s), 1660-1530 (br, m), 1451 (w) cm⁻¹.

Synthesis of end catalyst-functionalized SWNTs (7). The end norbornene-functionalized SWNTs (5) (51 mg), benzylidene-bis(tricyclohexylphosphine)dichlororuthenium catalyst (6) (20.0 mg, 2.4×10^{-2} mmol), and heptane (10.0 mL) were added into a 25 mL flask. The suspension was sonicated for 5 min and then stirred at room temperature for 12 h. The product was isolated by filtration through a 200 nm-pore diameter Teflon membrane, followed by washing with methanol (200 mL), CH₂Cl₂ (200 mL), and hexanes (200 mL). The recovered residue was then dried under vacuum overnight. The resulting SWNT macroinitiator was isolated as a black powder (54 mg). IR (KBr pellet): $\nu = 2937$ (s), 2860 (m), 1741 (m), 1660 (w), 1451 (w), 1204 (w) cm⁻¹.

General procedure for ring-opening metathesis polymerization using the end catalyst-functionalized SWNT macroinitiator (7). Approximately 3.0 mg of the SWNT macroinitiator (7) was dispersed in 10 mL of CHCl₃ by sonication for 5 min. The suspension was degassed by bubbling with nitrogen for 5 min, and a solution of norbornene (0.5 g, 5.3×10^{-3} mol) in 5 mL of CHCl₃ was added.

The suspension was then stirred at room temperature for 5-180 min. The product was filtered through a 200 nm-pore diameter Teflon membrane, and washed with CH_2Cl_2 (300 mL), THF (300 mL), and methanol (100 mL). The recovered residue was then dried under vacuum overnight. IR (KBr pellet): $\nu = 2926$ (s), 2856 (m), 1741 (m), 1648 (w), 1467 (w), 969 (w) cm^{-1} . ^1H NMR (200 MHz, CDCl_3): δ 0.91-1.19 (br), 1.19-1.48 (br), 1.64-1.97 (br), 2.20-2.55 (br), 2.70-2.90 (br), 5.12-5.40 (m).

General procedure for cleavage of polynorbornene from the end polynorbornene-functionalized SWNTs (8). A sample of the end polynorbornene-functionalized SWNTs (8) (51.0 mg) was suspended in THF (50.0 mL) followed by the addition of ground KOH (0.2 g, 3.6 mmol) and 18-crown-6 (1.0 g, 3.8 mmol). The solution was then stirred at room temperature for 48 h. The reaction mixture was filtered through a 200 nm-pore diameter Teflon membrane, followed by washing with THF (250 mL). This resulted in a black residue, composed of SWNTs, remaining on the membrane, with the filtrate containing the cleaved polynorbornene. The filtrate was concentrated to approximately 2 mL and precipitated into hexanes (100 mL). The precipitate was then filtered and dried under vacuum overnight, allowing the recovery of the cleaved polynorbornene as a white solid (20 mg). IR (KBr pellet): $\nu = 2956$ -2837 (br, m), 1660-1567 (br, m), 1470-1420 (br, m), 1351 (m), 1281 (w), 1250 (w), 1109 (s), 967 (m), 840 (w) cm^{-1} . ^1H NMR (200 MHz, CDCl_3): δ 0.91-1.19 (br), 1.19-1.48 (br), 1.64-1.97 (br), 2.20-2.55 (br), 2.70-2.90 (br), 5.12-5.40 (m).

Synthesis of side-wall phenol-functionalized SWNTs (9). Shortened SWNTs (30 mg), octyl aldehyde (2 mL, 0.012 mol), and N-(4-hydroxyphenyl) glycine (50 mg, 3.0×10^{-4} mol) were dispersed in 50 mL of DMF in a 250 mL round bottom flask. The mixture was stirred at 130°C under Ar for 5 days with further addition of 50 mg (3.0×10^{-4} mol) aliquots of N-(4-hydroxyphenyl) glycine once every 24 h. At the end of this process, the product was collected by filtration through a 200 nm-pore Teflon membrane, and was then washed thoroughly with CH_2Cl_2 (200 mL), THF (100 mL), and methanol (50 mL), and finally dried at 50°C under vacuum overnight. IR (KBr pellet): $\nu = 3437$ (s), 2926-2855 (m), 1634 (s) cm^{-1} .

Synthesis of side-wall vinyl-functionalized SWNTs (10). Side-wall phenol-functionalized SWNTs (9) (20 mg) and DMF (10 mL) were added in a 25 mL flame dried flask and sonicated for 5 min. That was followed by the addition of acryloyl chloride (8.0 mL, 98 mmol). Then the suspension was stirred at 50°C for 24 h. Triethylamine (1.0 mL) was added during the stirring period drop by drop. At the end of this process, the product was collected by filtration through a 200 nm-pore Teflon membrane, and was then washed thoroughly with CH_2Cl_2 (300 mL) and methanol (300 mL), and finally dried at 50°C under vacuum overnight. IR (KBr pellet): $\nu = 2940$ -2883 (m), 1740 (s), 1663 (s), 1208 (s) cm^{-1} .

Synthesis of side-wall catalyst-functionalized SWNTs (11). The side-wall vinyl-functionalized SWNTs (10) (10 mg), benzylidene-bis(tricyclohexylphosphine)dichlororuthenium catalyst (6) (10.0 mg, 1.2×10^{-2} mmol), and heptane (10.0 mL) were added into a 25 mL flask. The suspension

was sonicated for 5 min and then stirred at room temperature for 12 h. The product was isolated by filtration through a 200 nm-pore diameter Teflon membrane, followed by washing with methanol (200 mL), CH_2Cl_2 (200 mL), and hexanes (200 mL). The recovered residue was then dried under vacuum overnight. The resulting SWNT macroinitiator was isolated as a black powder (9 mg). IR (KBr pellet): $\nu = 2925$ (s), 2856 (m), 1767 (m), 1662 (w), 1466 (w) cm^{-1} .

General procedure for ring-opening metathesis polymerization using the side-wall catalyst-functionalized SWNT macroinitiator (11). Approximately 3.0 mg of the side-wall SWNT macroinitiator (11) was dispersed in 10 mL of CHCl_3 by sonication for 5 min. The suspension was degassed by bubbling with nitrogen for 5 min, and a solution of norbornene (0.5 g, 5.3×10^{-3} mol) in 5 mL of CHCl_3 was added. The suspension was then stirred at room temperature for 5-180 min. The product was filtered through a 200 nm-pore diameter Teflon membrane, and washed with CH_2Cl_2 (300 mL), THF (300 mL), and methanol (100 mL). The recovered residue was then dried under vacuum overnight. IR (KBr pellet): $\nu = 2926$ (s), 2856 (m), 1741 (m), 1648 (w), 1467 (w), 969 (w) cm^{-1} . ^1H NMR (200 MHz, CDCl_3): δ 0.91-1.19 (br), 1.19-1.48 (br), 1.64-1.97 (br), 2.20-2.55 (br), 2.70-2.90 (br), 5.12-5.40 (m).

Chapter 4 Functionalization of SWNTs using Radical Chemistry

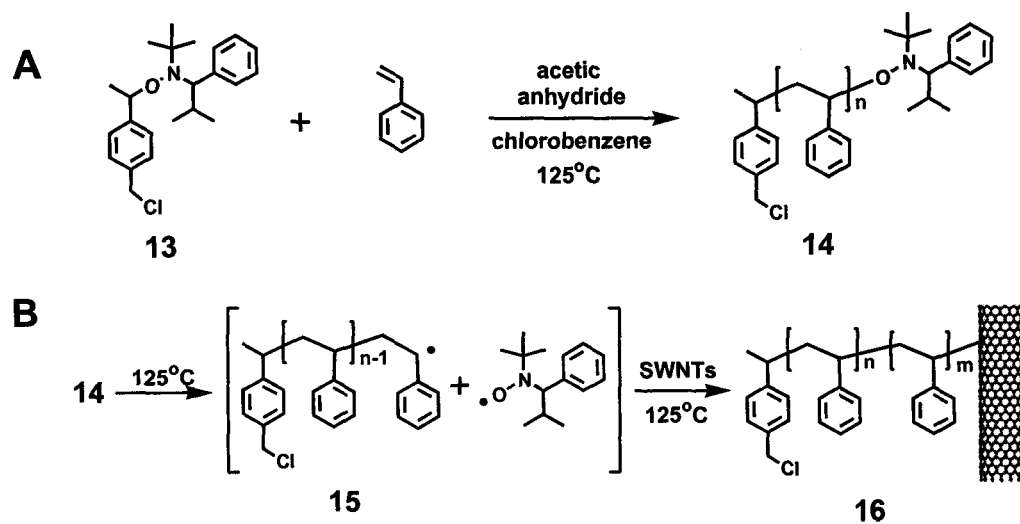
4.1 Overview

This project was initially conceived and developed by Zhaoling Yao in the Adronov's group, who synthesized the initial polystyrene (PS)-functionalized SWNTs using radical coupling. This preliminary work was then extended to the preparation of more composites, including PS and poly[(t-butyl acrylate)-b-styrene] (PtBA-b-PS) functionalized nanotubes, and fully characterized using techniques such as IR, Raman, NMR, UV/Vis, TEM, AFM, DSC and TGA. It was found that both PS-SWNT and PtBA-b-PS-SWNT composites were highly soluble in a variety of organic solvents. The t-butyl groups of appended PtBA-b-PS could be removed to produce poly[(acrylic acid)-b-PS]-functionalized carbon nanotubes (PAA-b-PS-SWNT) that became insoluble in regular organic solvents, but became soluble in a mixture of chloroform/methanol (v/v: 3/1). Furthermore, the PAA-b-PS-SWNT composite was found to form aggregates in a mixture of chloroform/methanol (v/v: 1/1), as determined by dynamic light scattering (DLS).

4.1.1 Functionalization of shortened SWNTs with PS

Nitroxide-terminated polystyrene (PS) samples were prepared by "living" free-radical polymerization utilizing one of the universal alkoxyamine unimolecular initiators recently introduced by Hawker and co-workers (Scheme 13A).⁸¹ By varying the styrene to initiator ratio, PS with designed molecular

weight and narrow polydispersity was prepared. The product was analyzed by gel permeation chromatography, measured against commercial PS standards. Figure 20 shows GPC results for the product. Its molecular weight was found to be 4901 g/mol with a polydispersity below 1.10. The SWNTs used in this study, produced by the HiPco process, were purchased from Carbon Nanotechnologies, Inc. We chose to shorten the as-received nanotubes by sonication in a mixture of $\text{HNO}_3/\text{H}_2\text{SO}_4$ to lengths of ca. 350 nm, in order to enhance the solubility of our desired nanotube-polymer conjugates.¹⁸



Scheme 13. (A) Preparation of PS by nitroxide mediated “living” free-radical polymerization and (B) Functionalization of SWNTs by nitroxide-terminated PS.

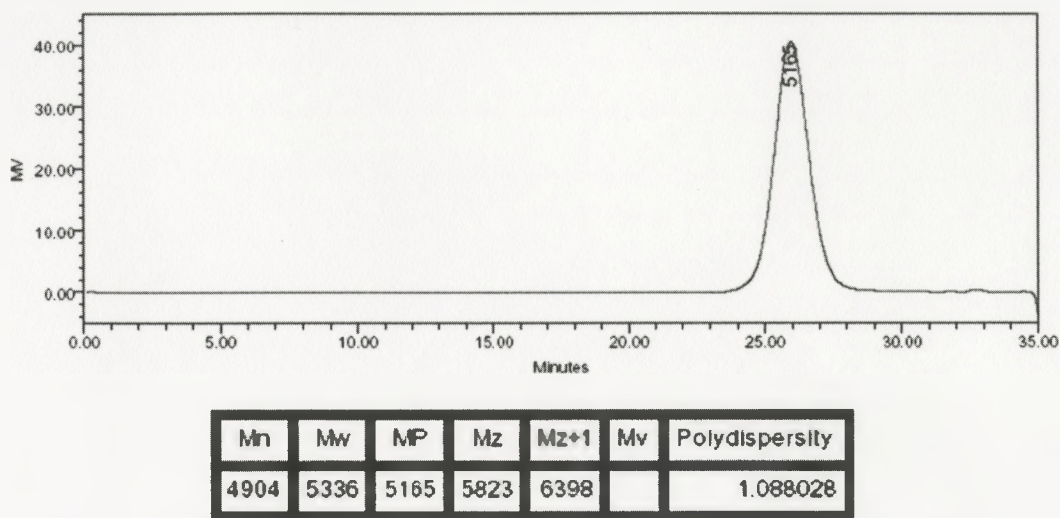


Figure 20. GPC results of a typical PS prepared by “living” free-radical polymerization utilizing alkoxyamine initiator.

The radical addition of PS to shortened SWNTs (Scheme 13B) was a repetition of Zhaoling Yao’s work. Details of this work will be available in her respective publications and Ph.D. thesis. It was found that the functionalization reaction drastically affected the solubility characteristics of the resulting PS-functionalized SWNTs (16). As illustrated in Figure 21A, the shortened SWNTs exhibit some solubility in water prior to polymer functionalization. However, after functionalization with PS, the composite (16) became insoluble in H₂O but highly soluble in a range of organic solvents, including CH₂Cl₂, THF, CHCl₃ and toluene (Figure 21B-D). The high solubility allowed further purification of the composites by simple column chromatography, through which we could observe a dark layer of silica containing our immobilized nanotube conjugates while all free polymer was removed when using CH₂Cl₂ as the eluent. Then the composite was

extracted from the dark silica using $\text{CH}_2\text{Cl}_2/\text{H}_2\text{O}$ (v/v:1/4). Then the organic layer was collected and solvent was evaporated in vacuo. A control experiment, in which the SWNTs were reacted with the alkoxyamine initiator (13) alone, under identical conditions and concentrations to the polymer reactions described above, resulted in no increase in the solubility of the resulting SWNTs. In this case, magic-angle spinning solid-state proton NMR provided some evidence that functionalization of the SWNTs with initiator fragments did occur (see Figure 22), but these structures were too small to impart any solubility difference to the SWNTs.

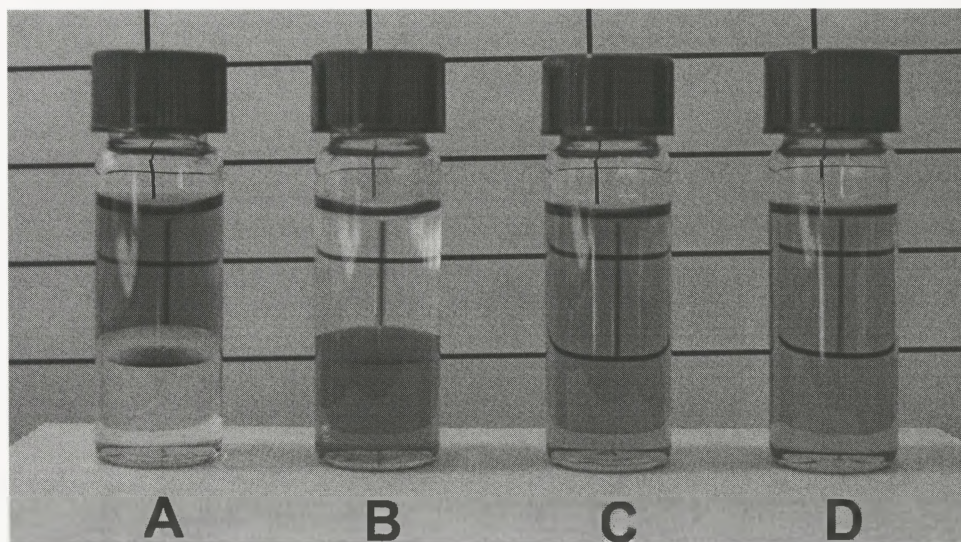


Figure 21. Shortened SWNTs in $\text{CH}_2\text{Cl}_2/\text{H}_2\text{O}$ (A) and PS functionalized SWNTs in various solvents: $\text{CH}_2\text{Cl}_2/\text{H}_2\text{O}$ (B), THF (C), CHCl_3 (D).

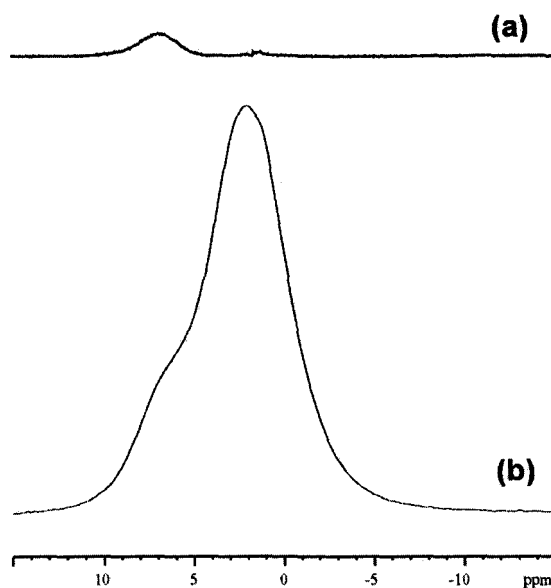


Figure 22. Solid-state ^1H NMR spectra of (a) shortened unfunctionalized SWNTs and (b) initiator-functionalized SWNTs.

The degree of SWNT solubility in various solvents as a result of functionalization could be estimated by UV/Vis spectroscopy following a procedure published by Smalley and Tour, who reported the specific extinction coefficient for HiPco SWNTs at 500 nm to be 0.028.⁷² We also measured the specific extinction coefficient of our shortened SWNTs to determine whether or not the shortening process has an effect on their absorption properties. Four different aqueous solutions of shortened SWNTs were prepared by dispersing small quantities of the nanotubes and thoroughly sonicating for 10 minutes. Any insoluble residues were allowed to settle for 48 h before collecting supernatant samples for absorption measurements, which were performed using a Cary 50 UV/Vis absorption spectrometer and 10 mm path-length cuvettes. These

solutions were visually inspected for optical clarity prior to measurement. Subsequently, 50.0 mL aliquots of each sample were placed on a hot plate, and the solvent was evaporated by gentle heating under a stream of N₂. This was followed by vacuum drying at 50°C for 24 h before weighing the residue to determine the mass of solubilized SWNTs. The measured absorption was then plotted against nanotube concentration, and the slope of the linear-least-squares fit of the data was found to be 0.0139, with an R-squared value of 0.996 (shown in Figure 23). This slope is analogous to the extinction coefficient of Beer's law, and can be used to estimate the concentration of nanotube solutions. It should be noted that the non-zero intercept indicates some loss of light, likely due to scattering from the relatively large nanotube structures in solution. Our measured specific extinction coefficient is significantly lower than that reported by Smalley and Tour, indicating that shorter, more oxidized nanotubes are less efficient absorbers of light than pristine, full-length nanotubes. This value was used to determine the concentration of the polymer functionalized nanotube samples in various organic solvents. The highest solubility was found to be in THF, with nanotube concentrations in excess of 600 mg/L for all the synthesized samples. Figure 24B shows the UV/Vis absorbance of PS-SWNTs in THF which is very similar to the spectrum of shortened SWNTs shown in Figure 24A.

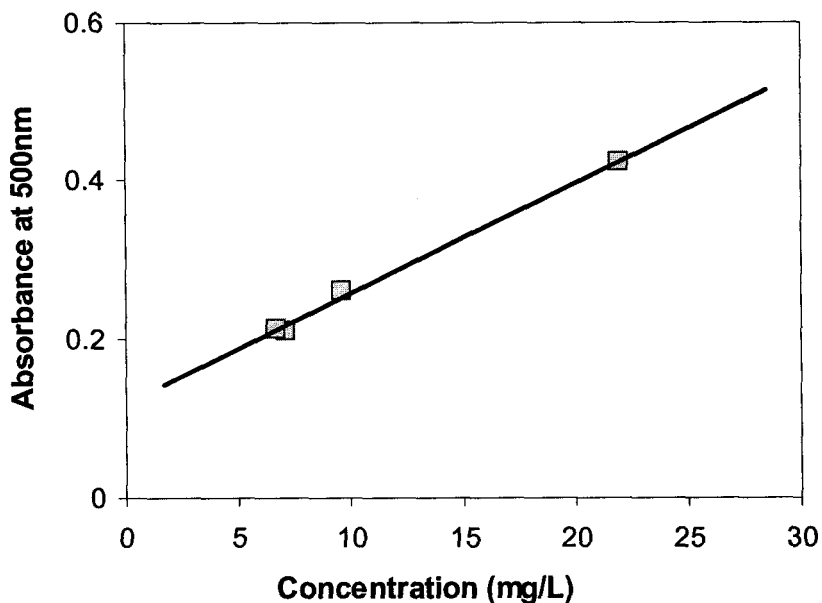


Figure 23. Optical density at 500 nm of shortened SWNTs in H₂O at different concentrations. The straight line is a linear-least-squares fit to the data; slope = 0.0139.

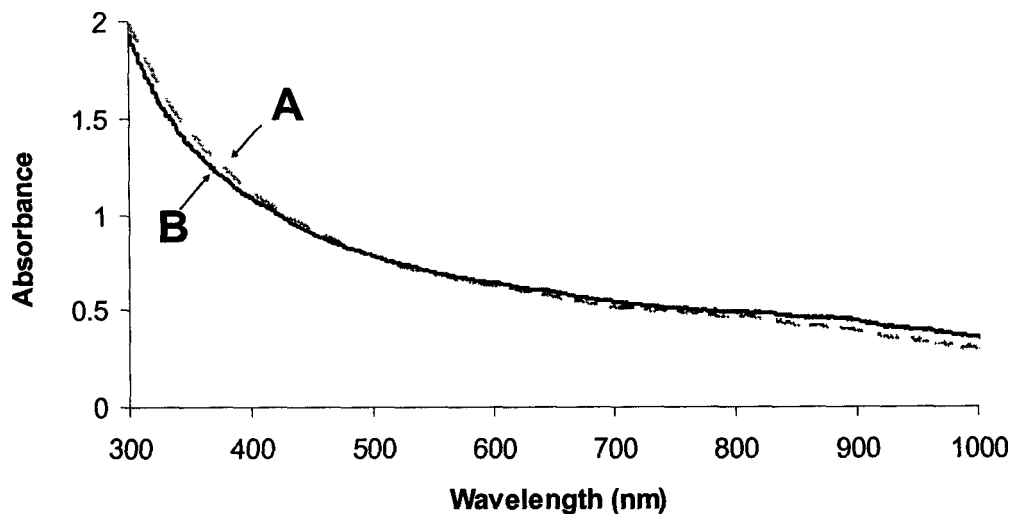


Figure 24. UV/Vis spectra of (A) shortened SWNTs in H₂O and (B) PS functionalized SWNTs in THF (normalized to the absorbance at 500 nm).

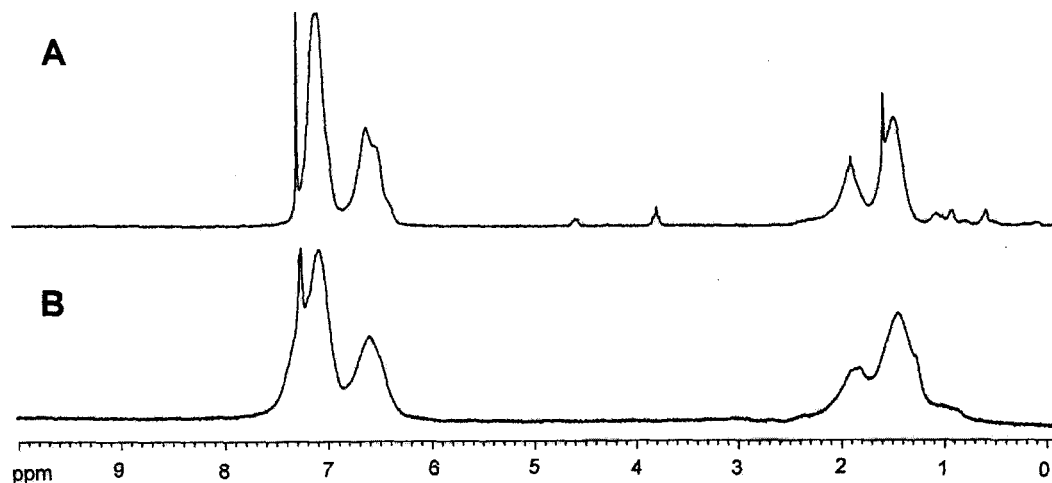


Figure 25. ^1H NMR spectra of (A) PS and (B) PS functionalized SWNTs.

Due to this relatively high solubility, solution-phase ^1H NMR spectroscopy could be utilized to study the polymer portion of the sample. Figure 25 depicts the ^1H NMR spectra of the PS sample used in nanotube functionalization and the PS-functionalized SWNTs (**16**). The two spectra are nearly identical, clearly illustrating that PS was, indeed, attached to the surface of carbon nanotubes. Both of the spectra show the expected aromatic signals for PS, at $\delta = 7.07$ and 6.56 ppm (broad), as well as the backbone signals at $\delta = 1.84$ and 1.42 ppm. The relatively small peaks below 1.0 ppm in Figure 25A are due to the alkoxyamine initiator fragments at the ends of the polymer chains. These signals remain after functionalization (Figure 25B), indicating that some nitroxide radical fragments may have also coupled to the SWNTs during the course of the reaction.

The PS-SWNT composite and shortened SWNTs were additionally analyzed by Raman spectroscopy and both exhibited the characteristic nanotube absorptions at ca. 190-260 and 1550-1590 cm^{-1} , corresponding to the radial breathing modes (RBM) and the tangential G mode of the SWNTs, respectively (Figure 26). Previous studies have shown that the observed RBM frequencies are inversely proportional to nanotube diameter,^{93,94} allowing the determination of nanotube diameter distributions within samples. Interestingly, a decrease in the amount of larger diameter nanotubes was observed after functionalization, indicating that smaller diameter nanotubes may be more reactive toward the radical chemistry that was carried out as part of this work. Others have also observed diameter-selective reactivity in both sidewall and defect-site functionalization reactions,^{95,96} attributing the higher reactivity of lower-diameter tubes to π -orbital misalignment and pyramidalization strain energy, both of which are inversely proportional to tube diameter.⁹⁷ Differences in the tangential G mode before and after the radical functionalization can also be seen from the Raman data. Here, the diameter-dependent Breit-Wigner-Fano (BWF) peak, seen as a close shoulder to the higher frequency, diameter independent Lorentzian peak at 1585 cm^{-1} prior to functionalization (Figure 26A), shifts to lower frequency after functionalization (Figure 26B). This shift is consistent with previous observations of direct proportionality between the frequency of the BWF peak and nanotube diameter.⁹⁸ Again, this lends evidence to the fact that the radical coupling reaction is selective for lower-diameter nanotubes. In addition, the

broad disorder peak at approximately 1320 cm^{-1} is present in both spectra and corresponds to the presence of sp^3 -hybridized carbon atoms within the nanotubes. The relative intensity of this peak seems to decrease after polymer functionalization, but the exact cause of this decrease in the number of sp^3 hybridized carbon atoms within the lower-diameter nanotubes is unknown. Overall, the Raman results indicate that, although the nanotube solubility has increased dramatically as a result of the functionalization, the chemical structure of the SWNTs has mainly been preserved.

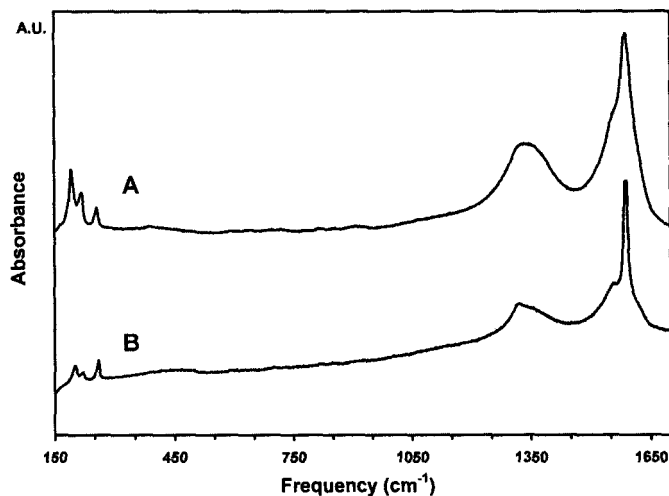


Figure 26. Raman spectra of (A) shortened SWNTs and (B) PS functionalized SWNTs.

Analysis of the PS functionalized SWNTs by AFM revealed that the topological morphology of these materials is significantly altered when compared to unfunctionalized SWNTs. Figure 27A depicts a sample of shortened SWNTs

prior to functionalization, prepared by spin casting from a DMF suspension onto freshly cleaved mica, where small nanotube bundles having heights in the range of 1-5 nm can be observed. After polymer functionalization, the nanotube sample was spin cast from a THF solution, again onto freshly cleaved mica, and revealed nanotube bundles that were coated or closely associated with an amorphous material, presumably PS (Figure 27B). In this sample, individual features reached heights of up to 15 nm. Interestingly, changing the casting solvent to CHCl_3 resulted in a completely different surface topology, where the nanotube bundles seemed to be embedded in a polymeric matrix (Figure 27C). It is presumed that differences in the nanotube-polymer vs. nanotube-solvent interactions are responsible for the observed topological differences (SWNTs have been shown to be more soluble in CHCl_3 than in THF). TEM analysis of the PS functionalized structures also revealed the presence of nanotube bundles coated with amorphous *polymeric material* (Figure 27D).

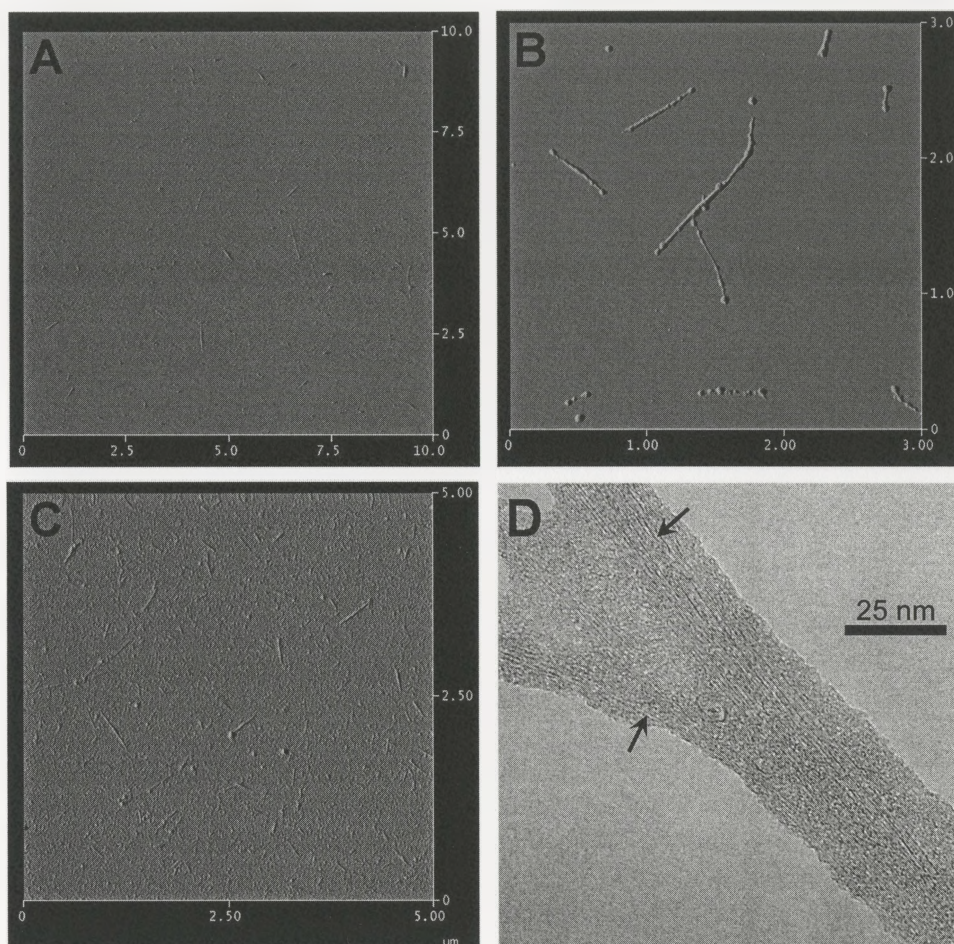


Figure 27. AFM image of purified SWNTs (A); AFM image of PS functionalized SWNTs spin-cast from THF solution (B); AFM image of PS functionalized SWNTs spin-cast from CHCl_3 solution (C); TEM image of PS functionalized SWNTs (D).

The polymer-functionalized SWNTs were also studied by thermogravimetric analysis (TGA). The TGA traces for both the starting PS and the grafted nanotubes are shown in Figure 28. The PS sample completely decomposes in the temperature range between 365 and 450°C. Although the PS-

functionalized nanotube sample exhibits a very similar decomposition curve, the mass loss stops at approximately 13% and remains stable to 800°C, indicating that the sample was composed of 13% nanotubes by weight. Interestingly, the onset of decomposition in the nanotube sample is at slightly lower temperature, possibly due to the high thermal conductivity of the SWNTs in the sample.

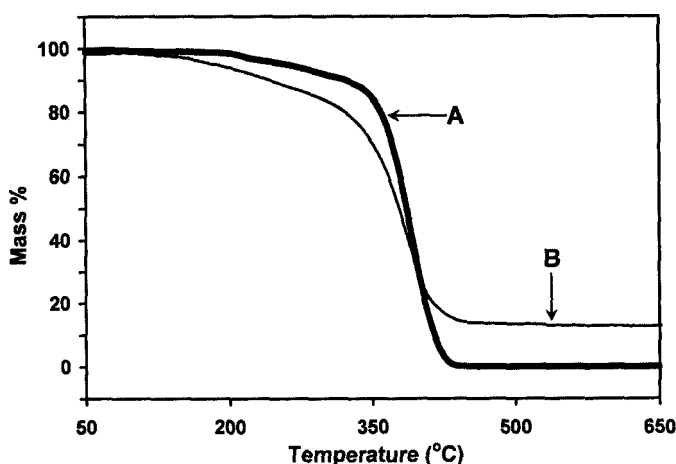


Figure 28. TGA traces of (A) PS and (B) PS functionalized SWNTs.

4.1.2 Functionalization of shortened SWNTs with Diblock Copolymers.

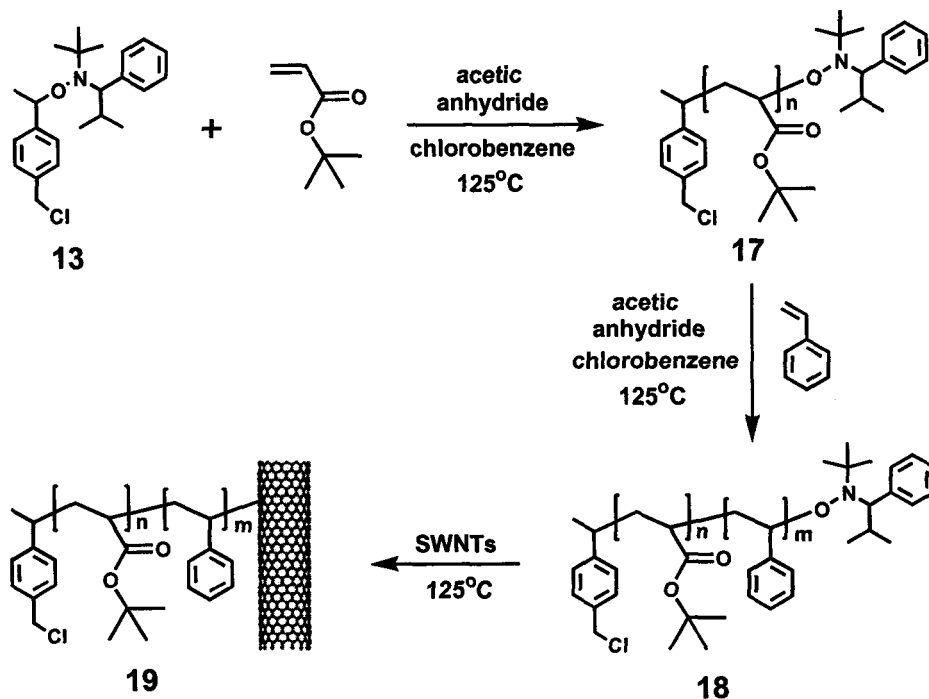
Taking advantage of the synthetic control provided by nitroxide-mediated radical polymerization, we were able to prepare diblock copolymers composed of a poly(*t*-butyl acrylate) block and a polystyrene block (PtBA-*b*-PS), as depicted in Scheme 14. The resulting diblock copolymer **18** had a molecular weight of 18,000 g/mol and a PDI of 1.40, determined by GPC against polystyrene

standards. ^1H NMR indicated that the monomer ratio of tBA to styrene in the product was approximately 1:2.5. Coupling of the polystyrene block to shortened SWNTs was performed according to the aforementioned procedure at 125°C and resulted in block copolymer functionalized SWNTs **19** (Scheme 14).

The block-copolymer functionalized SWNTs were also found to be highly soluble in various organic solvents, including THF, CH_2Cl_2 , and CHCl_3 , with concentrations of SWNTs exceeding 200 mg/L (based on the calculated specific extinction coefficient from Figure 23). Comparing the solution ^1H NMR spectra of the block copolymer and the copolymer-functionalized SWNTs (Figure 29), it is clear that the two spectra are nearly identical. Considering that any free polymer can easily be removed by filtration, and its absence can be determined by TLC, the similarity of these NMR spectra is indicative of nanotube functionalization with the block copolymer.

TGA analysis also confirmed that the block copolymer functionalization had occurred. Figure 30A illustrates the TGA traces for the bulk PtBA-b-PS (i) and the PtBA-b-PS-functionalized SWNTs (ii). For this block copolymer, two decomposition events are clearly visible, with the first one at ca. 200°C attributed to the loss of the t-butyl groups in the PtBA block (~25% mass loss), and the second being the depolymerization of the remaining polymer. The nanotube-attached polymer decomposes in a virtually identical manner, again confirming its composition, but does not reach a complete mass loss above 450°C . The remaining mass, approximately 38%, gives an indication of the nanotube content

in the original sample. Clearly, the relatively high nanotube content in this sample, as compared to the polystyrene-functionalized sample (16), indicates that the functionalization step was less efficient, and also partly explains the decreased solubility of this material. Again, this sample exhibits a slightly decreased onset of decomposition for both steps, similar to what was observed for the homopolymer (Figure 28). This phenomenon may be due to the increased thermal conductivity imparted to the material due to the presence of SWNTs.



Scheme 14. Preparation of PtBA-b-PS by nitroxide mediated “living” free-radical polymerization, and its utilization for the functionalization of SWNTs.

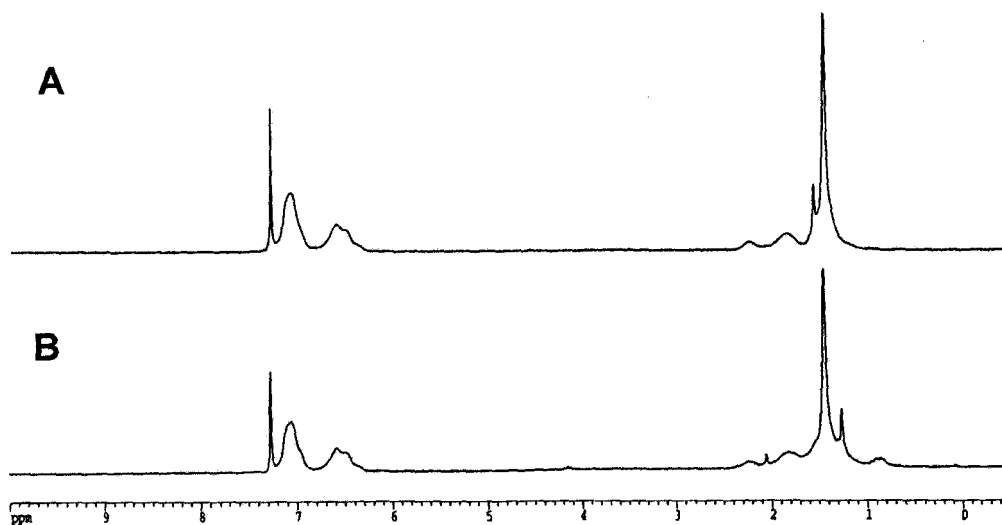


Figure 29. ^1H NMR spectra of (A) PtBA-b-PS and (B) PtBA-b-PS functionalized SWNTs.

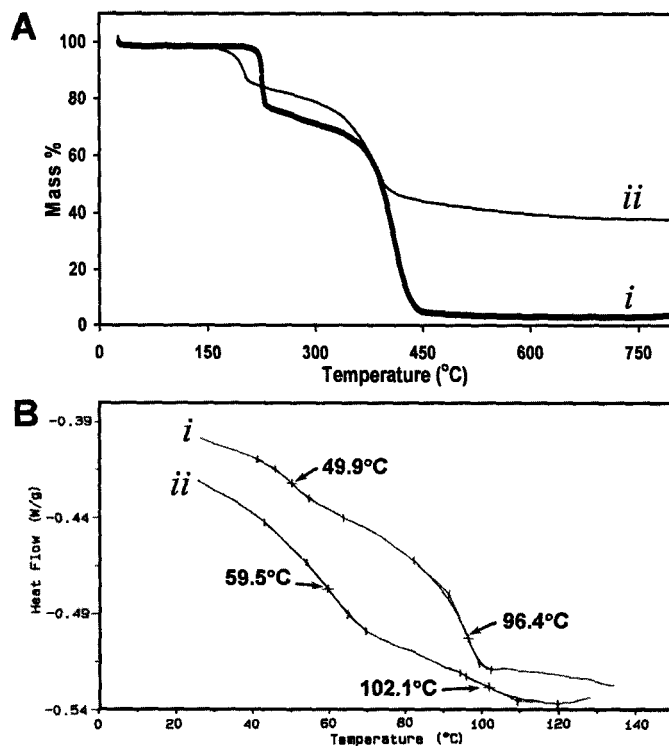


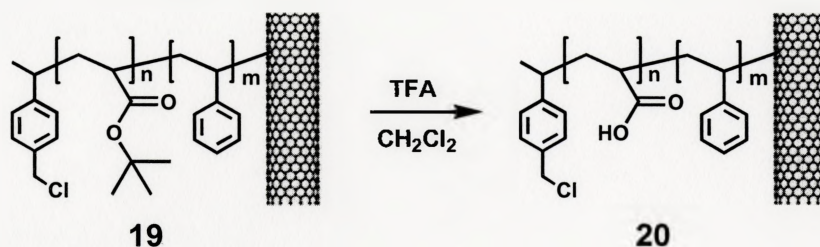
Figure 30. TGA data (A) and DSC data (B) for PtBA-b-PS (i) and PtBA-b-PS functionalized SWNTs (ii).

It is also possible to measure the glass transition temperature (T_g) for each of the two polymer blocks within bulk PtBA-*b*-PS and PtBA-*b*-PS-functionalized SWNTs via differential scanning calorimetry (DSC) analysis. Figure 30B shows the DSC traces for the block copolymer and the polymer-functionalized SWNTs. Our previous work has shown that constraint of polymer chains due to their attachment to nanotube surfaces results in an increase in the T_g .⁹⁰ The same effect also occurred in this case, where attachment of PtBA-*b*-PS chains to the nanotube surface constrains their mobility, resulting in an observed 9°C increase for the tBA block and a 6°C increase for the styrene block.

4.1.3 SWNTs Functionalized with Amphiphilic Block Copolymers

Previous work in the Adronov's group has shown that removal of the *t*-butyl groups of poly(*t*-butyl acrylate) functionalized SWNTs drastically affects their solubility properties.¹⁸ Along similar lines, the *t*-butyl groups within the nanotube-attached PtBA-*b*-PS polymer could be removed by treating the sample with a 20% trifluoroacetic acid (TFA)/CH₂Cl₂ solution (v/v) for 12 h.¹⁸ Upon evaporation of the solvent and acid, the resulting poly(acrylic acid)-block-polystyrene (PAA-*b*-PS) functionalized SWNTs (**20**) were found to be completely insoluble in organic solvents such as THF and CH₂Cl₂, but also insoluble in pure H₂O and CH₃OH. However, this sample was soluble in mixtures of chloroform and methanol of various composition. Interestingly, changes in polymer

morphology as a result of changing the solvent composition could be observed. For example, Figure 31A depicts the ^1H NMR spectrum of the PAA-b-PS-functionalized SWNTs solution in a 3/1 mixture of $\text{CDCl}_3/\text{CD}_3\text{OD}$ (v/v) where both the acrylic acid and styrene blocks dissolve very well. The aromatic signals for the styrene block are clearly visible at $\delta = 6.91$ and 6.43 ppm (broad). Aliphatic proton signals were also observed in the region between 0.8 and 2.3 ppm, corresponding to the polymer backbone protons for both blocks. The signals at $\delta = 1.69$ and 3.56 ppm are due to traces of THF left from the deprotection process that were difficult to remove, even after prolonged heating under vacuum. However, when the deuterated methanol portion of the solvent was increased to a $\text{CDCl}_3/\text{CD}_3\text{OD}$ ratio of 1:1, the ^1H NMR of the sample exhibited significant changes (Figure 31B). In this case, both the aromatic and aliphatic signals corresponding to the PS block dramatically decreased in intensity, while the signals corresponding to the PAA block remained practically unchanged. This behaviour is indicative of a contraction and rigidification of the PS block (Figure 31, cartoon), making it less mobile and thereby dramatically increasing the relaxation time of the protons associated with it. It should be noted that this behaviour is completely reversible, where evaporation of the solvent and re-uptake in a 3/1 $\text{CDCl}_3/\text{CD}_3\text{OD}$ mixture reproduces the ^1H NMR trace shown in Figure 31A.



Scheme 15. Deprotection of PtBA-b-PS functionalized SWNTs to produce PAA-b-PS functionalized SWNTs.

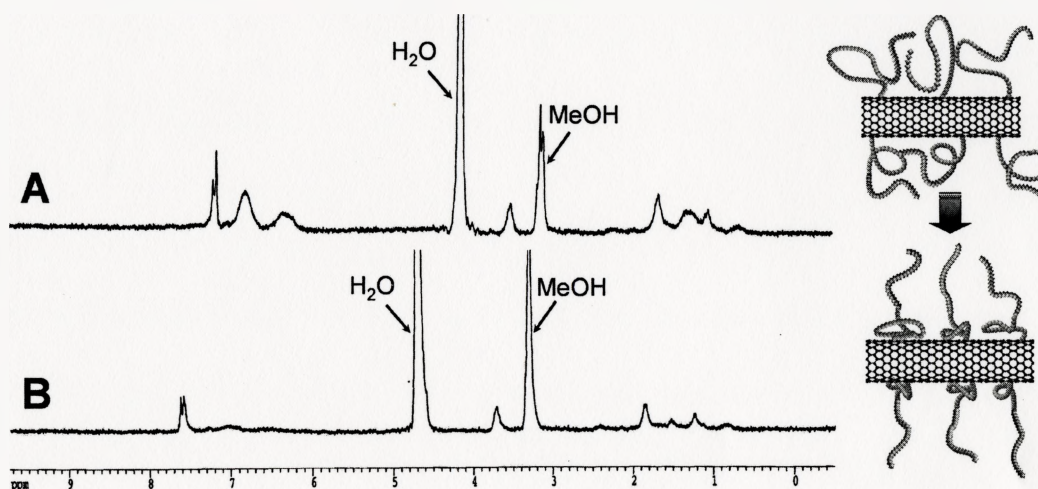


Figure 31. ^1H NMR spectra of (A) PAA-b-PS functionalized SWNTs in $\text{CDCl}_3/\text{CD}_3\text{OD}$ (v/v: 3/1) and (B) PAA-b-PS functionalized SWNTs in $\text{CDCl}_3/\text{CD}_3\text{OD}$ (v/v: 1/1).

Dynamic Light Scattering (DLS) was also utilized to determine the size distributions of the block copolymer-functionalized SWNTs. In the case of the nanotubes functionalized with the amphiphilic block copolymer, the observed diameter of the material was again found to vary with solvent composition.

Starting with the relatively nonpolar solvent mixture containing 6/1 CHCl₃/MeOH, the light scattering measurement indicated a hydrodynamic diameter of 164 nm. Considering that the average length of the nanotubes, as measured by AFM, is approximately 300 nm, the DLS data seems to indicate that, in solution, the polymer-functionalized nanotubes are still flexible enough to fold and adopt shapes that are more compact than would be expected from fully elongated structures. Interestingly, as the solvent composition was increased in polarity to a 1/1 and 1/2 CHCl₃/MeOH ratio, the measured hydrodynamic diameter increased to 302 and 712 nm, respectively (Figure 32). This data, along with the solution ¹H NMR data, is consistent with a contraction and rigidification of the polystyrene block, which may result in an overall rigidification and elongation of the SWNTs. Alternatively, the increased hydrodynamic diameter may be indicative of intermolecular aggregation between multiple polymer-functionalized SWNTs, especially in the most polar solvent system.

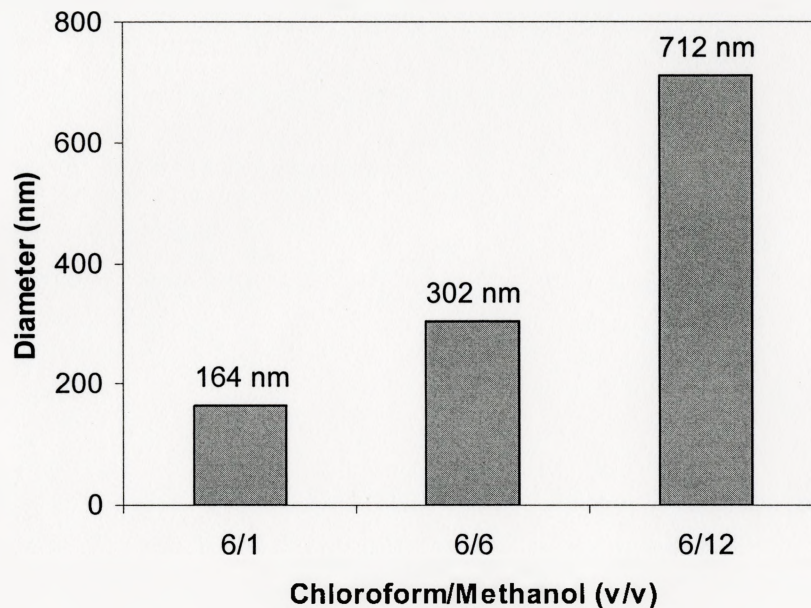


Figure 32. DLS data of PAA-b-PS functionalized SWNTs particles in $\text{CHCl}_3/\text{MeOH}$.

4.2 Experimental

General. Single-walled carbon nanotubes (SWNTs) were purchased from Carbon Nanotechnologies, Inc. (Houston, TX). Styrene and t-butyl acrylate were purified by passing through basic alumina and stored in the fridge. All other reagents and solvents were purchased from commercial suppliers and used as received. Raman spectra were obtained using a Renishaw InVia Raman Microscope equipped with an 1800 grooves/mm grating, CCD detector and He-Ne Laser (632.8 nm). Atomic Force Microscopy was done using a Digital Instruments NanoScope IIIa Multimode AFM, with samples prepared by

spincoating sample solutions or suspensions on freshly cleaved mica substrates. The images were recorded with standard tips in tapping mode at a scan rate of 1.0 Hz. TEM analysis was performed using a Philips CM12 operating at 120 keV. NMR was performed on a Bruker 200 MHz instrument in CDCl₃. Filtration was done through either a 100 nm-pore polycarbonate membrane (Millipore) or a 200 nm-pore teflon membrane (Millipore). Polymer molecular weight and polydispersity index (PDI) were estimated by gel permeation chromatography (GPC) using a Waters 2695 Separations Module equipped with a Waters 2996 Photodiode Array Detector, a Waters 2414 Refractive Index Detector, a Waters 2475 Multi λ Fluorescence Detector, and four Polymer Labs PLgel individual pore size columns. Polystyrene standards were used for calibration, and tetrahydrofuran (THF) was used as the eluent at a flow rate of 1.0 mL/min. Differential scanning calorimetry (DSC) was performed on a TA 2100 Modulated Differential Scanning Calorimeter with a temperature gradient of 15 degrees/min. The concentrations of the soluble polymer functionalized SWNTs were calculated from UV/Vis absorption spectra measured using a Cary 50 UV/Vis Spectrophotometer. Thermogravimetric analysis (TGA) was carried out on a NETZSCH STA 409 PC instrument under Ar with a temperature range from 20°C to 800°C and a temperature gradient of 5 degrees/min. Particle sizing was conducted by dynamic light scattering. A Lexel 95 ion laser operating at a wavelength of 514 nm was used as the light source, and data were analyzed using

a BI-9000AT digital autocorrelator, version 6.1 (Brookhaven Instruments Corp.).

The light scattering was measured at 90°.

Shortening and Purification of SWNTs. A 250 mL flask charged with 50 mg of SWNTs and 100 mL of a H₂SO₄/HNO₃ (v/v: 3/1) solution was sonicated for 2 hours. The mixture was then diluted with 200 mL of distilled water. After cooling to room temperature, the diluted solution was filtered through a 100 nm-pore polycarbonate membrane. The black material collected from the membrane was further treated by stirring with 50 mL H₂SO₄/H₂O₂ (9/1) in a 250 mL flask for 30 min at room temperature. Another 50 mL of H₂SO₄/H₂O₂ (9/1) was added and the solution was sonicated for 5 min. After dilution using 200 mL of distilled water, the solution was filtered through a 100 nm-pore polycarbonate membrane. The resulting mat of SWNTs was washed thoroughly using first a 10 mM NaOH solution, and then distilled water until the pH of the filtrate was 7.

Synthesis of polystyrene (14). In a typical reaction, a 25 mL round-bottom flask was charged with styrene (4.0 mL, 35.0 mmol), alkoxyamine initiator (13) (288 mg, 0.77 mmol), and acetic anhydride (0.03 mL, 0.32 mmol). The mixture was bubbled with N₂ for 30 min and then the flask was placed into a 125°C oil bath. The reaction was allowed to proceed for 12 h and the product was dissolved in CH₂Cl₂ and then precipitated by dropwise addition of the solution into methanol. The precipitate was filtered and then dried at 50°C under vacuum overnight. The product was analyzed by GPC. ¹H NMR (200MHz, CDCl₃): δ 7.08 (broad), 6.59 (broad), 1.90 (broad), and 1.49 (broad) ppm.

Synthesis of poly(t-butyl acrylate) (PtBA) (17). In a typical reaction, a 25 mL round-bottom flask was charged with t-butyl acrylate (3.0 mL, 20.4 mmol), alkoxyamine initiator (**13**) (176 mg, 0.47 mmol), acetic anhydride (0.05 mL, 0.53 mmol) and chlorobenzene (2.0 mL). The mixture was bubbled with N₂ for 30 min and then the flask was placed into a 125°C oil bath. The reaction was allowed to proceed for 12 h and the product was dissolved in THF and then precipitated by dropwise addition of the solution into methanol/H₂O (v/v: 1/1). The precipitate was filtered and then dried at 50°C under vacuum overnight. The product was analyzed by GPC, resulting in a M_n = 5898 g/mol and a PDI=1.62. ¹H NMR (200MHz, CDCl₃): δ 2.21 (broad), 1.82 (broad), and 1.42 (broad) ppm.

Synthesis of poly[(t-butyl acrylate)-b-styrene] (PtBA-b-PS) (18). In a typical reaction, a 25 mL round-bottom flask was charged with styrene (3 mL, 26.0 mmol), 1.5 g of poly(t-butyl acrylate) (M_n = 5898 g/mol), acetic anhydride (0.05 mL, 0.53 mmol) and chlorobenzene (3.0 mL). The mixture was bubbled with N₂ for 30 min and then the flask was placed into a 125°C oil bath. The reaction was allowed to proceed for 12 h and the product was dissolved in THF and then precipitated by dropwise addition of the solution into methanol. The precipitate was filtered and then dried at 50°C under vacuum overnight. The product was analyzed by GPC, resulting in a M_n = 18000 g/mol and a PDI=1.40. ¹H NMR (200MHz, CDCl₃): δ 7.03 (broad), 6.56 (broad), 2.20 (broad), 1.82 (broad), and 1.42 (broad) ppm.

Synthesis of PtBA-b-PS functionalized SWNTs (19). In a typical reaction, 10 mg of purified SWNTs, 0.05 mL (0.53 mmol) of acetic anhydride and 500 mg of PtBA-b-PS ($M_n = 18226$ g/mol) were dispersed in 15 mL of DMF in a 50 mL flask. The mixture was bubbled with N_2 for 30 min and then was stirred at 125°C under argon for 3 days. The product was collected by filtering through a 200 nm-pore Teflon membrane while washing thoroughly with CH_2Cl_2 , THF, and methanol, and then dried at 50°C under vacuum overnight. The mass of the isolated product increased by approximately 50%. ^1H NMR (200MHz, CDCl_3): δ 7.05 (broad), 6.58 (broad), 2.20 (broad), 1.82 (broad), 1.44 (broad), and 0.88 (broad) ppm.

Formation of poly(acrylic acid-b-styrene) (PAA-b-PS) functionalized SWNTs (20). In a typical reaction, 8.0 mg of PtBA-b-PS functionalized SWNTs, 1.0 mL of trifluoroacetic acid (TFA) and 5.0 mL of CH_2Cl_2 were dispersed in 15 mL of DMF in a 25 mL flask. The mixture was stirred at room temperature for 6 h. Then the solvent and excess TFA were evaporated in vacuo. The product was dried at 50°C under vacuum overnight. ^1H NMR (200MHz, $\text{CDCl}_3/\text{CD}_3\text{OD}$ (v/v: 3/1)): δ 6.91 (broad), 6.43 (broad), 2.22 (broad), 1.70 (broad), 1.30 (broad), 1.09 (broad), and 0.71 (broad) ppm.

Chapter 5 Conclusions

We have demonstrated that it is possible to functionalize shortened SWNTs with ruthenium alkylidene catalysts by utilizing the acid groups formed at the ends and defect sites of nanotubes as a result of the shortening process, and the phenol groups on side walls formed via 1,3-dipolar cycloaddition. The catalyst-functionalized nanotubes are effective initiators of norbornene polymerization. The polymerizations were shown to result in the formation of polynorbornene-functionalized nanotubes, which had a slightly improved solubility in organic solvents. The polymer molecular weights were shown to increase linearly with time, and the polydispersities were found to be consistent with expected values for the catalysts used. Future work will involve the attachment of “third-generation” ruthenium-based olefin metathesis catalysts that will result in narrower polydispersities, and will allow for the preparation of block copolymers.

One simple strategy for the functionalization of carbon nanotubes with well-defined polymers was successfully carried out. It allows for the introduction of numerous functional and architecturally complex polymer structures, such as block copolymers, onto the surface of SWNTs. Such polymer-functionalized carbon nanotubes acquire drastically improved solubility, and the PAA-b-PS functionalized carbon nanotubes have exhibited their self-assembly properties, which will impact on their future technological applicability.

References:

- (1) Iijima, S. *Nature* **1991**, *354*, 56-58.
- (2) Iijima, S.; Ichihashi, T. *Nature* **1993**, *363*, 603-605.
- (3) Avouris, P. *Acc. Chem. Res.* **2002**, *35*, 1026-1034.
- (4) Collins, P. G.; Avouris, P. *Scientific American* **2000**, *283*, 62-69.
- (5) Dai, H. J. *Acc. Chem. Res.* **2002**, *35*, 1035-1044.
- (6) Ajayan, P. M. *Chem. Rev.* **1999**, *99*, 1787-1799.
- (7) Choi, W. B.; Chung, D. S.; Kang, J. H.; Kim, H. Y.; Jin, Y. W.; Han, I. T.; Lee, Y. H.; Jung, J. E.; Lee, N. S.; Park, G. S.; Kim, J. M. *Appl. Phys. Lett.* **1999**, *75*, 3129-3131.
- (8) Ebbesen, T. W.; Ajayan, P. M. *Nature* **1992**, *358*, 220-222.
- (9) Bethune, D. S.; Kiang, C. H.; de Vries, M. S.; Gorman, G.; Savoy, R.; Vazquez, J.; Beyers, R. *Nature* **1993**, *363*, 605-607.
- (10) Thess, A.; Lee, R.; Nikolaev, P.; Dai, H.; Petit, P.; Robert, J.; Xu, C.; Lee, Y. H.; Kim, S. G.; Rinzler, A. G.; Colbert, D. T.; Scuseria, G. E.; Tomanek, D.; Fischer, J. E.; Smalley, R. E. *Science* **1996**, *273*, 483-487.
- (11) Journet, C.; Maser, W. K.; Bernier, P.; Loiseau, A.; Chapelle, M. L.; Lefrant, S.; Deniard, P.; Lee, R.; Fischer, J. E. *Nature* **1997**, *388*, 756-758.
- (12) Niyogi, S.; Hamon, M. A.; Hu, H.; Zhao, B.; Bhowmik, P.; Sen, R.; Itkis, M. E.; Haddon, R. C. *Acc. Chem. Res.* **2002**, *35*, 1105-1113.
- (13) Hirsch, A. *Angew. Chem. Int. Edit.* **2002**, *41*, 1853-1859.
- (14) Bahr, J. L.; Tour, J. M. *J. Mater. Chem.* **2002**, *12*, 1952-1958.
- (15) Liu, J.; Rinzler, A. G.; Dai, H. J.; Hafner, J. H.; Bradley, R. K.; Boul, P. J.; Lu, A.; Iverson, T.; Shelimov, K.; Huffman, C. B.; Rodriguez-Macias, F.; Shon, Y. S.; Lee, T. R.; Colbert, D. T.; Smalley, R. E. *Science* **1998**, *280*, 1253-1256.
- (16) Chen, J.; Hamon, M. A.; Hu, H.; Chen, Y.; Rao, A. M.; Eklund, P. C.; Haddon, R. C. *Science* **1998**, *282*, 95-98.

- (17) Sun, Y. P.; Fu, K. F.; Lin, Y.; Huang, W. J. *Acc. Chem. Res.* **2002**, *35*, 1096-1104.
- (18) Yao, Z.; Braid, N.; Botton, G. A.; Adronov, A. *J. Am. Chem. Soc.* **2003**, *125*, 16015-16024.
- (19) Liu, Y.; Adronov, A. *Macromolecules* **2004**, *37*, 4755-4760.
- (20) Qin, S.; Qin, D.; Ford, W.T.; Resasco, D.E.; Herrera, J. E. *J. Am. Chem. Soc.* **2004**, *126*, 170-176.
- (21) Qin, S.; Qin, D.; Ford, W.T.; Resasco, D.E.; Herrera, J. E. *Macromolecules* **2004**, *37*, 752-757.
- (22) Viswanathan, G.; Ajayan, P.M. *J. Am. Chem. Soc.* **2003**, *125*, 9258-9259.
- (23) Qin, S.; Qin, D.; Ford, W.T.; Herrera, J.E.; Resasco, D.E.; Bachilo, S.M.; Weisman, R.B. *Macromolecules* **2004**, *37*, 3965-3967.
- (24) Chopra, N. G. ; Luyken, H. ; Cherrey, K. ; Crespi, V.H. ; Cohen, M. L.; Louie, S.G.; Zettl, A. *Science* **1995**, *269*, 966-968.
- (25) Fan, S.; Chapline, M. G.; Franklin, N. R.; Tomblor, T. W.; Cassell, A. M.; Dai, H. *Science* **1999**, *283*, 512-514.
- (26) Ivanov, V.; Nagy, J. B.; Lambin, P.; Lucas, A.; Zhang, X. B.; Zhang, X. F.; Bernaerts, D.; Van Tendeloo, G.; Amelinckx, S.; Van Landuyt, J. *Chem. Phys. Lett.* **1994**, *223*, 329-335.
- (27) Ren, Z. F.; Huang, Z. P.; Xu, J. W.; Wang, J. H.; Bush, P.; Siegal, M. P.; Provencio, P. N. *Science* **1998**, *282*, 1105-1107.
- (28) Pan, Z. W.; Xie, S. S.; Chang, B. H.; Wang, C. Y.; Lu, L.; Liu, W.; Zhou, W. Y.; Li, W. Z.; Qian, L. X. *Nature* **1998**, *394*, 631-632.
- (29) Terrones, M.; Grobert, N.; Olivares, J.; Zhang, J. P.; Terrones, H.; Kordatos, K.; Hsu, W. K.; Hare, J. P.; Townsend, P. D.; Prassides, K.; Cheetham, A. K.; Kroto, H. W.; Walton, D. R. M. *Nature* **1997**, *388*, 52-55.
- (30) Jose-Yacaman, M.; Miki-Yoshida, M.; Rendon, L.; Santiesteban, T. G. *Appl. Phys. Lett.* **1993**, *62*, 202-204.

- (31) Nikolaev, P.; Bronikowski, M. J.; Bradley, R. K.; Rohmund, F.; Colbert, D. T.; Smith, K. A.; Smalley, R. E. *Chem. Phys. Lett.* **1999**, *313*, 91-97.
- (32) Li, F.; Cheng, H. M.; Bai, S.; Su, G.; Dresselhaus, M. S. *Appl. Phys. Lett.* **2000**, *77*, 3161-3163.
- (33) Yu, M. F.; Files, B. S.; Arepalli, S.; Ruoff, R. S. *Phys. Rev. Lett.* **2000**, *84*, 5552-5555.
- (34) Hone, J.; Batlogg, B.; Benes, Z.; Johnson, A. T.; Fischer, J. E. *Science* **2000**, *289*, 1730-1733.
- (35) Wong, E. W.; Sheehan, P. E.; Lieber, C. M. *Science* **1997**, *277*, 1971-1975.
- (36) Falvo, M. R.; Clary, C. J.; Taylor, R. M.; Chi, V.; Brooks, F. P.; Washburn, S.; Superfine, R. *Nature* **1997**, *389*, 582-584.
- (37) Heer, W. A.; Chatelain, A.; Ugaarte, D. A. *Science* **1995**, *270*, 1179-1180.
- (38) Tans, S.; Verschueren, A.; Dekker, C. *Nature* **1998**, *393*, 49-52.
- (39) Collins, P. G.; Arnold, M. S.; Avouris, P. *Science* **2001**, *292*, 706-709.
- (40) Kong, J.; Franklin, N. R.; Zhou, C.; Chapline, M. G.; Peng, S.; Cho, K.; Dai, H. *Science* **2000**, *287*, 622-625.
- (41) Collins, P. G.; Bradley, K.; Ishigami, M.; Zettl, A. *Science* **2000**, *287*, 1801-1804.
- (42) Balaboine, F.; Schultz, P.; Richard, C.; Mallouh, V.; Ebbesen, T. W.; Mioskowski, C. *Angew. Chem. Int. Ed.* **1999**, *38*, 1912.
- (43) Hu, J.; Odom, T. W.; Lieber, C. M. *Acc. Chem. Res.* **1999**, *32*, 435-445.
- (44) Banerjee, S.; Wong, S. S. *Nano Lett.* **2002**, *2*, 49-53.
- (45) Banerjee, S.; Wong, S. S. *J. Am. Chem. Soc.* **2002**, *124*, 8940-8948.
- (46) Haremza, J. M.; Hahn, M. A.; Krauss, T. D. *Nano Lett.* **2002**, *2*, 1253-1258.
- (47) Banerjee, S.; Wong, S. S. *Nano Lett.* **2002**, *2*, 195-200.
- (48) Azamian, B. R.; Coleman, K. S.; Davis, J. J.; Hanson, N.; Green, M. L. H. *Chem. Commun.* **2002**, 366-367.

- (49) Baker, S. E.; Cai, W.; Lasseter, T. L.; Weidkamp, K. P.; Hamers, R. J. *Nano Lett.* **2002**, *2*, 1413-1417.
- (50) Dwyer, C.; Guthold, M.; Falvo, M.; Washburn, S.; Superfine, R.; Erie, D. *Nanotechnology* **2002**, *13*, 601-604.
- (51) Shim, M.; Kam, N. W. S.; Chen, R. J.; Li, Y.; Dai, H. *Nano Lett.* **2002**, *2*, 285-288.
- (52) Pompeo, F.; Resasco, D. E. *Nano Lett.* **2002**, *2*, 369-373.
- (53) Huang, W.; Taylor, S.; Fu, K.; Lin, Y.; Zhang, D.; Hanks, T., W.; Rao, A. M.; Sun, Y.-P. *Nano Lett.* **2002**, *2*, 311-314.
- (54) Pantarotto, D.; Partidos, C. D.; Graff, R.; Hoebeke, J.; Briand, J.-P.; Prato, M.; Bianco, A. *J. Am. Chem. Soc.* **2003**, *125*, 6160-6164.
- (55) Sun, Y.-P.; Huang, W.; Lin, Y.; Fu, K.; Kitaygorodskiy, A.; Riddle, L. A.; Yu, Y. J.; Carroll, D. L. *Chem. Mater.* **2001**, *13*, 2864-2869.
- (56) Mickelson, E. T.; Huffman, C. B.; Rinzler, A. G.; Smalley, R. E.; Hauge, R. H.; Margrave, J. L. *Chem. Phys. Lett.* **1998**, *296*, 188-194.
- (57) Georgakilas, V.; Kordatos, K.; Prato, M.; Guldi, D. M.; Holzinger, M.; Hirsch, A. *J. Am. Chem. Soc.* **2002**, *124*, 760-761.
- (58) Georgakilas, V.; Tagmatarchis, N.; Pantarotto, D.; Bianco, A.; Briand, J. P.; Prato, M. *Chem. Commun.* **2002**, 3050-3051.
- (59) Bahr, J. L.; Yang, J. P.; Kosynkin, D. V.; Bronikowski, M. J.; Smalley, R. E.; Tour, J. M. *J. Am. Chem. Soc.* **2001**, *123*, 6536-6542.
- (60) Holzinger, M.; Vostrowsky, O.; Hirsch, A.; Hennrich, F.; Kappes, M.; Weiss, R.; Jellen, F. *Angew. Chem. Int. Edit.* **2001**, *40*, 4002-4005.
- (61) Tang, Z.; Xu, H. *Macromolecules* **1999**, *32*, 2569-2576.
- (62) Curran, S. A.; Ajayan, P. M.; Blau, W. J.; Carroll, D. L.; Coleman, J. N.; Dalton, A. B.; Davey, A. P.; Drury, A.; McCarthy, B.; Maier, S.; Strevens, A. *Adv. Mater.* **1998**, *10*, 1091-1093.

- (63) Star, A.; Stoddart, F. J.; Steuerman, D.; Diehl, M.; Boukai, A.; Wong, E. W.; Yang, X.; Chung, S.-W.; Choi, H.; Heath, J. R. *Angew. Chem. Int. Edit.* **2001**, *40*, 1721-1725.
- (64) Star, A.; Liu, Y.; Grant, K.; Ridvan, L.; Stoddart, F. J.; Steuerman, D.; Diehl, M. R.; Boukai, A.; Heath, J. R. *Macromolecules* **2003**, *36*, 553-560.
- (65) Steuerman, D. W.; Star, A.; Narizzano, R.; Choi, H.; Ries, R. S.; Nicolini, C.; Stoddart, J. F.; Heath, J. R. *J. Phys. Chem. B* **2002**, *106*, 3124-3130.
- (66) Chen, J.; Liu, H. Y.; Weimer, W. A.; Halls, M. D.; Waldeck, D. H.; Walker, G. C. *J. Am. Chem. Soc.* **2002**, *124*, 9034-9035.
- (67) Chen, R. J.; Zhang, Y.; Wang, D.; Dai, H. *J. Am. Chem. Soc.* **2001**, *123*, 3838-3839.
- (68) Gomez, F. J.; Chen, R. J.; Wang, D. W.; Waymouth, R. M.; Dai, H. *J. Chem. Commun.* **2003**, 190-191.
- (69) Nakashima, N.; Tomonari, Y.; Murakami, H. *Chem. Lett.* **2002**, 638-639.
- (70) Riggs, J. E.; Guo, Z. X.; Carroll, D. L.; Sun, Y. P. *J. Am. Chem. Soc.* **2000**, *122*, 5879-5880.
- (71) Hill, D. E.; Lin, Y.; Rao, A. M.; Allard, L. F.; Sun, Y. P. *Macromolecules* **2002**, *35*, 9466-9471.
- (72) Sano, M.; Kamino, A.; Okamura, J.; Shinkai, S. *Langmuir* **2001**, *17*, 5125-5128.
- (73) Wu, W.; Zhang, S.; Li, Y.; Li, J. X.; Liu, L. Q.; Qin, Y. J.; Guo, Z. X.; Dai, L. M.; Ye, C.; Zhu, D. B. *Macromolecules* **2003**, *36*, 6286-6288.
- (74) Lin, Y.; Zhou, B.; Fernando, K. A. S.; Liu, P.; Allard, L. F.; Sun, Y. P. *Macromolecules* **2003**, *36*, 7199-7204.
- (75) Louie, J.; Grubbs, R. H. *Organometallics* **2002**, *21*, 2153-2164.
- (76) Love, J. A.; Morgan, J. P.; Trnka, T. M.; Grubbs, R. H. *Angew. Chem. Int. Edit.* **2002**, *41*, 4035-4037.
- (77) Choi, T. L.; Grubbs, R. H. *Angew. Chem. Int. Edit.* **2003**, *42*, 1743-1746.

- (78) Juang, A.; Scherman, O. A.; Grubbs, R. H.; Lewis, N. S. *Langmuir* **2001**, *17*, 1321-1323.
- (79) Kim, N. Y.; Jeon, N. L.; Choi, I. S.; Takami, S.; Harada, Y.; Finnie, K. R.; Girolami, G. S.; Nuzzo, R. G.; Whitesides, G. M.; Laibinis, P. E. *Macromolecules* **2000**, *33*, 2793-2795.
- (80) Gomez, F. J.; Chen, R. J.; Wang, D. W.; Waymouth, R. M.; Dai, H. J. *Chem. Commun.* **2003**, 190-191.
- (81) Benoit, D.; Chaplinski, V.; Braslau, R.; Hawker, C. J. *J. Am. Chem. Soc.* **1999**, *121*, 3904-3920.
- (82) Georges, M. K.; Veregin, R. P. N.; Kazmaier, P. M.; Hamer, G. K.; Saban, M. *Macromolecules* **1994**, *27*, 7228-7229.
- (83) Malmstrom, E. E.; Miller, R. D.; Hawker, C. J. *Tetrahedron* **1997**, *53*, 15225-15236.
- (84) Hawker, C. J.; Bosman, A. W.; Harth, E. *Chem. Rev.* **2001**, *101*, 3661.
- (85) M. Prato, *J. Mater. Chem.* **1997**, *7*, 1097-1109.
- (86) Shaffer, M. S. P.; Koziol, K. *Chem. Commun.*, **2002**, 2074-2075.
- (87) Barraza, H. J.; Pompeo, F.; O'Rear, E. A.; Resasco, D. E. *Nano Lett.* **2002**, *2*, 797-802.
- (88) Rao, A. M.; Richter, E.; Bandow, S.; Chase, B.; Eklund, P. C.; Williams, K. A.; Fang, S.; Subbaswamy, K. R.; Menon, M.; Thess, A.; Smalley, R. E.; Dresselhaus, G.; Dresselhaus, M. S. *Science* **1997**, *275*, 187-191.
- (89) Bahr, J. L.; Mickelson, E. T.; Bronikowski, M. J.; Smalley, R. E.; Tour, J. M. *Chem. Commun.* **2001**, 193-194.
- (90) Finkelshtein, E. S.; Makovetskii, K. L.; Yampol'skii, Y. P.; Portnykh, E. B.; Ostrovskaya, I. Y.; Kaliuzhnyi, N. E.; Pritula, N. A.; Gol'berg, A. I.; Yatsenko, M. S.; Platé, N. A. *Makromol. Chem.* **1991**, *192*, 1-9.
- (91) Savin, D. A.; Pyun, J.; Patterson, G. D.; Kowalewski, T.; Matyjaszewski, K. *J. Polym. Sci., Part B: Polym. Phys.* **2002**, *40*, 2667-2676.

- (92) Bahr, J. L.; Tour, J. M. *Chem. Mater.* **2001**, *13*, 3823-3824.
- (93) Bachilo, S. M.; Strano, M. S.; Kittrell, C.; Hauge, R. H.; Smalley, R. E.; Weisman, R. B. *Science* **2002**, *298*, 2361-2366.
- (94) Strano, M. S.; Doorn, S. K.; Haroz, E. H.; Kittrell, C.; Hauge, R. H.; Smalley, R. E. *Nano Lett.* **2003**, *3*, 1091-1096.
- (95) Huang, W. J.; Fernando, S.; Lin, Y.; Zhou, B.; Allard, L. F.; Sun, Y. P. *Langmuir* **2003**, *19*, 7084-7088.
- (96) Banerjee, S.; Wong, S. S. *Nano Lett.* **2004**, *4*, in press.
- (97) Chen, Z.; Thiel, W.; Hirsch, A. *ChemPhysChem* **2003**, *4*, 93-97.
- (98) Jorio, A.; Souza, A. G.; Dresselhaus, G.; Dresselhaus, M. S.; Swan, A. K.; Unlu, M. S.; Goldberg, B. B.; Pimenta, M. A.; Hafner, J. H.; Lieber, C. M.; Saito, R. *Phys. Rev. B* **2002**, *65*, 155412-155420.